Correspondence to:

A. Filippova,
afilippova@geomar.de

Authigenic and Detrital Carbonate Nd Isotope Records Reflect Pulses of Detrital Material Input to the Labrador Sea During the Heinrich Stadials

Alexandra Filippova[1] ⓘ**, Martin Frank[1]** ⓘ**, Markus Kienast[2]** ⓘ**, Marcus Gutjahr[1]** ⓘ**, Ed C. Hathorne[1]** ⓘ**, and Claude Hillaire-Marcel[3]** ⓘ

[1]GEOMAR Helmholtz Centre for Ocean Research Kiel, Kiel, Germany, [2]Dalhousie University, Halifax, NS, Canada, [3]University of Quebec Montreal, Montreal, QC, Canada

Abstract Limited constraints on the variability of the deep-water production in the Labrador Sea complicate reconstructions of the strength of the Atlantic Meridional Overturning Circulation (AMOC) during the Late Quaternary. Large volumes of detrital carbonates were repeatedly deposited in the Labrador Sea during the last 32 kyr, potentially affecting radiogenic Nd isotope signatures. To investigate this the Nd isotope compositions of deep and intermediate waters were extracted from the authigenic Fe-Mn oxyhydroxide fraction, foraminiferal coatings, the residual silicates and leachates of dolostone grains. We provide a first order estimation of Nd release via dissolution of detrital carbonates and its contribution to the authigenic ε_{Nd} signatures in the Labrador Sea. During the Last Glacial Maximum the Nd isotope signatures in the Labrador Sea would allow active water mass mixing with more radiogenic ε_{Nd} values (−12.6 and −14) prevailing in its eastern part whereas less radiogenic values ($\varepsilon_{Nd} \sim -18.4$) were found on the western Labrador slope. The deposition of detrital carbonates during Heinrich stadials (2,1) was accompanied by negative detrital and authigenic Nd isotope excursions ($\varepsilon_{Nd} \sim -31$) that were likely controlled by dissolution of dolostone or dolostone associated mineral inclusions. This highly unradiogenic signal dominated the authigenic phases and individual water masses in the Labrador Sea, serving as potential source of highly unradiogenic Nd to the North Atlantic region, while exported southward. The Holocene authigenic ε_{Nd} signatures of the coatings and leachates significantly differed from those of the detrital silicates, approaching modern bottom water mass signatures during the Late Holocene.

Plain Language Summary The Labrador Sea is an important region for deep water formation and for the ocean circulation in the Atlantic region. Over the last 32 thousand years, numerous discharges from melting glaciers added freshwater to the Labrador Sea which could help understand the future effects of current melting glaciers. This information is necessary to better constrain climate predictions in order to gauge the effects on the Global Ocean Water Circulation. However, past deep water production in the Labrador is still poorly constrained, complicating reconstruction of the Atlantic Meridional Overturning Circulation on different timescales. In this study we investigated changes in deep and intermediate water mass circulation patterns over the last 32 kyr based on the radiogenic Nd isotope compositions that serve as a water mass circulation proxy. Analysis of four marine sediment cores show that the deposition of large volumes of detrital carbonates during studied period had a large effect on the recorded in the sediment column signals. New data suggest active water mass circulation during the maximum extent of glacial ice sheets. The modern day ocean circulation patterns have emerged during the Late Holocene (6 ka).

1. Introduction

The Atlantic Meridional Overturning Circulation (AMOC) plays an important role in regional and global climate variability. Driven by the heat exchange between the atmosphere and the ocean its surface branch transports heat from equatorial regions to high latitudes thereby affecting the climate in the entire Northern Hemisphere (cf., Dickson et al., 1988; Dommenget & Latif, 2002; Gulev et al., 2001). Many studies have focused on the processes controlling present and past Atlantic deep water convection and water mass formation to improve our understanding of the factors driving AMOC variability and to achieve more realistic climate predictions (Chen et al., 2012; Dickson & Brown, 1994; Hall & Qu, 2006; McCarthy et al., 2015; Trouet et al., 2012; Vellinga & Wood, 2002).

The Labrador Sea plays a crucial role in the modification of North Atlantic Deep Water (NADW), which is transported southwards as a part of the Western Boundary Undercurrent (WBUC) (Dickson & Brown, 1994; Lacan & Jeandel, 2005; Lucotte & Hillaire-Marcel, 1994; Yashayaev & Clark, 2006; Yashayaev & Loder, 2009). The upper layer of NADW largely consists of Labrador Sea Water (LSW), which is produced by winter convection (Kieke & Yashayaev, 2014; Yashayaev & Clark, 2006). The intermediate and bottom layers of NADW originate in the Nordic Seas and spill over the Iceland Scotland Ridge (termed North East Atlantic Deep Water, NEADW) and across the Denmark Strait (termed Denmark Strait Overflow Water (DSOW) or North West Atlantic Bottom Water (NWABW) in paleoceanographic studies (Bilodeau et al., 1994)). In addition, the inflow of waters from the Arctic Ocean via the Canadian Arctic Archipelago (CAA) and a warm and saline inflow of North Atlantic Current (NAC) waters into the southern Labrador Sea contribute to the Labrador Current (LC). Labrador current flows southward along the Labrador Sea shelf and slope, the Newfoundland shelf and further along the eastern coast of Canada at depths between 400 and 1,200 m (Lazier & Wright, 1993). The present-day circulation in the Labrador Sea exhibits significant variability in intermediate and deep-water formation on decadal and annual time scales (Fisher et al., 2010; Khatiwala et al., 2002; Lazier, 1980; Yashayaev & Loder, 2009).

A range of proxies have been applied to reconstruct the presence of different NADW components and variable circulation patterns in the Labrador Sea on glacial/interglacial and millennial time scales during the Late Quaternary. Based on analysis of the clay mineralogy and $^{230}Th_{excess}$ data in a sediment core from Orphan Knoll in the southern Labrador Sea it has been suggested that the WBUC has been a persistent feature in the Labrador Sea over the last 25 kyr but was weaker during the Last Glacial Maximum (LGM) and Heinrich events (Fagel et al., 1996, 1997, 1999; Innocent et al., 1997; Veiga-Pires & Hillaire-Marcel, 1999). A recent study on benthic and planktonic foraminifera from Labrador Sea sediments found evidence for a strong glacial Subpolar Gyre and active boundary current regime during the LGM followed by enhanced convection during the early deglaciation (Seidenkrantz et al., 2021). Variations of the mean grain size of the detrital silt fraction and of the sedimentation rates show an increase in WBUC velocities at the beginning of the deglaciation reaching maximum speed between 10 ka and 9 ka (Balsam & Heusser, 1976; Haskell et al., 1991; Ledbetter & Balsam, 1985). Bilodeau et al. (1994) suggested the gradual establishment of the North East Atlantic Deep Water between 12 and 8.5 ka based on increased abundance of the benthic foraminiferal species *Epistominella exigua*, which was followed by the inception of Denmark Strait Overflow Water formation at ∼ 8.5 ka. This is consistent with reconstructions of Fagel et al. (2002, 2004), who found no indication of DSOW presence prior to 8.6 ka based on radiogenic Nd and Pb isotope compositions of the clay fraction. However, a study by Seidenkrantz et al. (2021) reported conditions comparable to the modern configuration in the deep Labrador Sea as early as 15 ka, potentially related to stronger overflow from the Greenland-Scotland Ridge. Different timings have been inferred for the initiation of the modern circulation in the Labrador Sea ranging from 14.3 ka based on Sm/Nd ratios and Nd isotope signatures of the carbonate free clay size fraction (Fagel et al., 1999) to ages not older than 10.3 ka (Innocent et al., 1997), 7.4 ka (Lochte, Repschläger, Seidenkrantz, et al., 2019) or even as late as 5.5 ka (Bilodeau et al., 1994).

During the Last Glacial Maximum the Labrador Sea was surrounded by extensive ice sheets (Figure 1), draining melt water, ice rafted debris and reworked sediments into the Labrador basin (Bond et al., 1992). The Laurentide Ice Sheet (LIS) was the largest ice sheet in the Northern Hemisphere, covering the area of modern-day Canada from the Cordillera to the Arctic and Atlantic oceans (Denton & Hughes, 1981; Dyke et al., 2002; Winsborrow et al., 2004) with more than 117 major ice streams (Margold et al., 2015) draining into the Arctic Ocean, North Atlantic and Labrador Sea (Figure 1b). One of the major LIS ice streams, the Hudson Strait Ice Stream, was underlain by Ordovician-Devonian limestones and dolostones, and has been identified as the source of detrital carbonate (≥2/3 calcite Nuttin et al., 2015) in marine sediments of the Labrador basin (Andrews & Tedesco, 1992; Andrews et al., 1995, 1999; Hillaire-Marcel et al., 2007; Lewis et al., 2011; MacLean et al., 1986; Rashid et al., 2012). In contrast, the northern Baffin Bay ice streams produced sediment layers with a higher dolomite content (≥2/3 dolomite; Andrews et al., 2012; Simon et al., 2014). In the northernmost part of CAA the independent Innuitian Ice sheet (IIS) merged with the LIS during the LGM. The Innuitian Ice sheet was connected to the Greenland Ice sheet by a saddle above Nares Strait, which spread to the northeast and southwest, extending to the Arctic Ocean and Baffin Bay and reaching the shelf break in the south (Dyke, 1999, Dyke et al., 2002; England, 1999; England et al., 2006; Funder & Hansen, 1996; Funder et al., 2004; Weidick et al., 2004). It has been proposed that during major meltwater events caused by instabilities of the ice sheets surrounding the Labrador Sea, the AMOC may have been reduced or even shut down completely (Böhm et al., 2015; McManus et al., 2004). In this regard, the Labrador Sea is a critical location to study the interaction of ice sheet dynamics and ocean circulation,
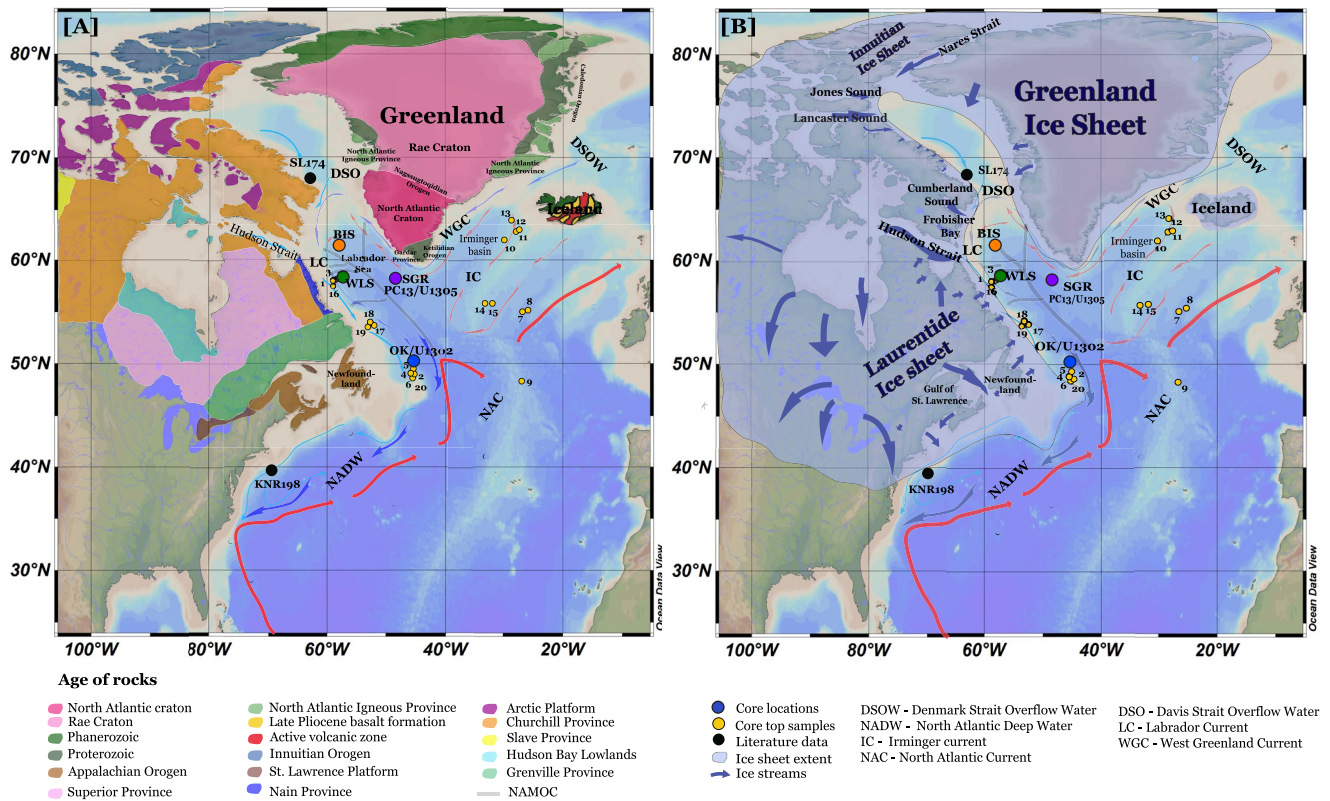
Figure 1. Schematic map of the study area. (a) Schematic representation of the water circulation in the Labrador Sea adopted from Yashayaev and Loder, (2016) Blue arrows represent cold deep currents and red arrows denote warm surface or subsurface currents. Color coded dots indicate the positions of the cores from this study. Yellow dots indicate locations of surface sediment samples from this study. Black dots represent core positions from published literature used for data comparison (U1302, U1305, Blaser et al., 2020; KNR198, Zhao et al., 2019). In color are shown different geological provinces of Canada (modified from Wheeler et al., 1996). Light gray lines denote the schematic position of Northwest Atlantic MidOcean Channel. (b) Last Glacial Maximum ice sheet extent with identified major ice streams (blue arrows). Map adopted from Margold et al., 2015, 2018). Acronyms are defined in Table S1. Map was produced using Ocean Data View (Schlitzer, 2015).

particularly with respect to LSW production intervals and to the glacial replacement of NADW by its shallower glacial analog, the Glacial North Atlantic Intermediate Water (GNAIW) (Böhm et al., 2015; Gutjahr et al., 2008; Howe, Piotrowski, Noble, et al., 2016).

Reconstructions of AMOC strength and geometry have mainly employed nutrient based and radiogenic isotope proxies but to date there is no clear consensus between these. Stable carbon isotope data from multiple studies suggest that Southern Source Water (SSW) filled the deep basins of the North Atlantic replacing the GNAIW during major cold events (Heinrich stadials) (Boyle & Keigwin, 1987; Duplessy et al., 1988; Oppo & Fairbanks, 1987; Thiagarajan et a., 2014). This is supported by studies based on the ε_{Nd} signatures of the authigenic fraction of marine sediments and of unclean foraminifera (Böhm et al., 2015; Gutjahr et al., 2008; Howe, Piotrowski, & Rennie, 2016; Lippold et al., 2016; Pahnke et al., 2008; Roberts et al., 2010). However, a growing number of studies on ε_{Nd} signatures of the authigenic fraction of marine sediments and foraminifera suggest reduced presence of SSW in the North Atlantic and a much larger fraction of Northern Source Water (NSW) in the intermediate and deep tropical North Atlantic Ocean during the LGM and deglaciation (Casme et al., 2003; Howe, Piotrowski, Noble, et al., 2016; Howe, Piotrowski, Oppo, et al., 2016, Howe et al., 2018; Huang et al., 2014; Pöppelmeier et al., 2020; Xie et al., 2012, 2014; Zhao et al., 2019). Recently published records of distinctly unradiogenic ε_{Nd} signatures prevailing during the early Holocene in areas within and outside of the Labrador Sea (Blaser et al., 2020; Howe, Piotrowski, & Rennie, 2016; Jaume-Segui et al., 2020; Pöppelmeier et al., 2018) were interpreted to result from either enhanced production of LSW (Roberts et al., 2010), enhanced partial dissolution of poorly chemically weathered detrital material deposited in the Labrador Sea following Laurentide Ice Sheet retreat (Blaser et al., 2020; Howe, Piotrowski, & Rennie, 2016; Pöppelmeier et al., 2018), or the admixture of a particularly dense water mass with highly unradiogenic Nd isotope composition to the abyssal

depths of the North Atlantic (Keigwin & Swift, 2017). Moreover, the most recent studies by Abbott et al. (2019) and Abbott et al. (2019, 2021) investigating the effect of benthic Rare Earth Elements (REE) fluxes and pore water exchange in marine sediments on regional and global scales, hypothesize that the ε_{Nd} signatures of marine authigenic fractions are almost entirely controlled by dissolution of the lithogenic material in pore waters and do not represent seawater signatures. Incubation experiments placing artificial Mn oxides in sediment cores from off the Frasier River estuary into isotopically enriched seawater revealed that some >80% of the Nd was sourced from pore waters (Patton et al., 2021) but such estuarine-coastal sediments are likely not representative of open marine sediments.

In this study we use radiogenic Nd isotope compositions extracted from the authigenic Fe-Mn oxyhydroxide fraction of bulk sediments and of chemically uncleaned (the Fe-Mn oxyhydroxide coatings were not removed prior to dissolution) mixed foraminifera in order to reconstruct the dissolved bottom water Nd isotope signatures present in the Labrador Sea over the last 32 kyr. These data are complemented by measurements of Nd isotope signatures of the detrital silicate fraction and progressive leaching of detrital carbonate-dolostone grains (Nd isotopes and REE) in order to constrain potential overprinting of the authigenic signal.

Radiogenic Nd isotopes, expressed in the ε_{Nd} notation due to small differences in $^{143}Nd/^{144}Nd$:

$$\varepsilon_{Nd} = \frac{\left(\frac{^{143}Nd}{^{144}Nd}sample\right) - \left(\frac{^{143}Nd}{^{144}Nd}CHUR\right)}{\frac{^{143}Nd}{^{144}Nd}CHUR} * 10000$$

where CHUR represents the present-day chondritic $^{143}Nd/^{144}Nd$ value of 0.512638 (Jacobssen & Wasserburg, 1980) are commonly used as a water mass circulation proxy (cf., Frank, 2002). The residence time of Nd in seawater lies between 200 and 1,000 years (Rempfer et al., 2011; Tachikawa et al., 2003), allowing different water mass provenances and mixing to be traced. Studies have demonstrated that radiogenic Nd signatures of authigenic phases in marine sediments can be from bottom seawater affected by boundary exchange processes (Jeandel, 2016) or altered after deposition via exchange with pore waters (Abbott et al., 2021). Although it seems Nd signatures of authigenic phases do not fully reflect seawater signatures, more work is needed to better understand their origin in different settings.

Based on leachate and foraminifera Nd isotope signatures of four new down core records combined with the dolostone (sedimentary carbonate rock, in which dolomite is the major mineral) leaching experiment data we decipher the nature of the authigenic signatures recorded in the Labrador Sea sediments over the past 32 kyr with a mean resolution of ~1 kyr and assess the extent of sedimentary overprinting based on analyses of total bulk sediment digests and dolostone grains.

2. Materials and Methods

2.1. Materials

Four sediment cores from the western and eastern parts of the Labrador Sea were used in this study. From the eastern Labrador Sea we sampled *Marion Dufresne* core MD99-2227 recovered from the southwest Greenland Rise, hereafter called South Greenland Rise core (SGR) (58° 12.38 N, 48° 22.22 W, 3,460 m) (Figure 1). The core location lies just below the high velocity axis of the modern Western Boundary Undercurrent (WBUC, Fagel et al., 2004). On the western side of the Labrador slope two cores were sampled. Core HU08-029-004, hereafter called Baffin Island shelf core (BIS) (61°27.49 N, 58°02.11 W, 2674 m) recovered off the southern Baffin Island shelf at a distance of approximately 180 km from the Hudson Strait shelf and core HU84-030-021, hereafter called Western Labrador Slope core (WLS) (58°22.06 N, 57°30.42 W, 2853 m) collected from the continental slope of the western Labrador Sea. All cores cover the Last Glacial Maximum (LGM), Heinrich Stadial (HS) 2 and 1, the Younger Dryas (YD) as well as the Holocene, with the exception of core SGR, which only covers the last 22 kyr. Core HU91-045-094, hereafter called Orphan Knoll core (OK) (50°12.26 N, 45°41.14 W, 3,448 m) recovered from the western Labrador Sea at Orphan Knoll is located in the transition zone between the North Atlantic Current and the Labrador Current.

The sedimentation rates vary between different locations. Cores on the western side (BIS, WLS, OK) tend to have high sedimentation rates (SR) during HS 2 and 1 ranging between 30 and 100 cm/kyr, and much lower during

Late Holocene (<20 cm/kyr), whereas off the southern tip of Greenland (SGR) SR were much higher during the Holocene (between 56 and 38 cm/kyr) and lower during HS1 (2 cm/kyr).

The original age models of the cores based on AMS ^{14}C ages were previously published by Fagel et al. (2004) for the SGR core, Gibb et al. (2014) for the BIS core, Hillaire-Marcel and de Vernal (1989) for the WLS core and Hillaire-Marcel et al. (1994) for the OK core. The original ages were recalibrated using the radiocarbon calibration program Calib 8.20 (Heaton et al., 2020; Stuiver & Reimer, 1993) and linearly interpolated between available AMS ^{14}C ages. A marine carbon reservoir age correction of 400 years was applied. The small age reversal observed for corrected ^{14}C ages (∼28 ka) in the OK core is a consequence of turbidity currents that disturbed the sediment between 410 and 470 cm (Hillaire-Marcel et al., 1994). Given that the two corrected ages have overlapping error bars for this interval they are considered to represent the same age.

Each core was sampled every 15–30 cm representing an approximate 1 kyr resolution, with the exception of the turbidite interval in core OK (between 414 and 454 cm). The Late Holocene sections in cores BIS and WLS were sampled at a lower resolution of 2–3 kyr due to lower sedimentation rates. In order to detect short-term variability, the sections containing the 8.2 ka event, the YD, and HS1 were sampled at higher resolution (every 10 cm corresponding to a resolution varying from ∼300 to ∼ 500 years). The reliability and the origin of the extracted authigenic Nd isotope signatures was tested by analyzing the Fe-Mn oxyhydroxide coatings of mixed uncleaned foraminifera from selected depth intervals (Table S2). Due to small sample sizes (3 g of sediment on average) and generally low abundances of foraminifera only 4 to 6 individual depths per core could be analyzed. The ε_{Nd} signatures of the authigenic Fe-Mn coating of marine sediments were compared with Nd isotope compositions of the residual silicate digests (Table S2). In addition, Nd isotope ratios were analyzed on dolostone grains picked from the same depth intervals as the foraminifera samples from all four sediment cores (Table S3).

To track the variability of the present-day bottom water masses along the flow path of the major inflows into the Labrador Sea additional surface sediment samples from the western coast of the Labrador Sea, near the Denmark Strait and along the Reykjanes Ridge were analyzed for Nd isotope compositions of the authigenic fractions and five samples of the residual silicate digests were analyzed following the same procedure described below (Table S2).

2.2. Methods

2.2.1. Sample Preparation and Mass Spectrometric Analysis

One to two g of the freeze-dried sediment were leached to extract the Nd isotope compositions of the authigenic fraction following an updated protocol of Gutjahr et al. (2007). Decarbonated surface sediment samples and SGR core samples showed more radiogenic ε_{Nd} signatures than modern seawater. To avoid bias arising from partial dissolution of basaltic glass particles abundant in the sediments proximal to Greenland and Iceland all samples in this study were not decarbonated prior to leaching. The validity of this method has been demonstrated by Blaser et al. (2016), who showed that the presence of carbonate in the samples yields more reliable paleo seawater results due to more efficient buffering of the pH of the leach solutions and also helps to reduce contamination with non-biogenic carbonates. The authigenic fraction was extracted during a one-hour leaching step using 25 ml of a diluted reducing and complexing solution consisting of 0.005 M hydroxylamine hydrochloride, 1.5% acetic acid and 0.03 M Na-EDTA buffered to pH of 3.6–3.8 using suprapure NaOH (∼0.035M) (cf., Blaser et al., 2016). The resulting supernatant was dried down, dissolved in concentrated nitric acid, dried down again, and transferred to Cl⁻ form by repeated dissolution in concentrated HCl. Finally, samples were dried down and re-dissolved in 1 M HCl/0.05 M HF loading solution for cation exchange column chemistry to purify Nd. For Nd separation from the sample matrix a set of two columns were used: cation columns with AG 50W-X8 resin (200–400 μm dry mesh) and columns loaded with Eichrom Ln-Spec resin with a bead size 50–100 μm for Nd (Pin & Zaldueguí, 1997). Cleaning of the foraminifera shells followed the procedure by Tachikawa et al. (2014). Briefly, freeze-dried sediment samples were washed through a >63 μm sieve and the remaining fraction was collected on a filter and dried. All planktonic and benthic foraminiferal shells present in the samples were handpicked, cracked until all chambers were opened and subsequently cleaned with ultra pure water (>18.2 MΩ) and ethanol to remove clays. The remaining sample was dissolved in 0.35 M acetic acid, centrifuged, the clear supernatant transferred into Teflon vials, dried down and re-dissolved in the loading solution for cation column chromatography following standard procedures. From the same sample fraction (>63 μm) detrital carbonate-dolostone grains (1–10 mg per grain) were picked when found, from all four sediment cores. Dolostone grains were first visually identified

based on color (gray, most common dolostone color), well defined structure and hardness. Some of the grains were tested with weak HCL (10%) acid for a reaction and Mg, Ca concentrations were measured in the solution in order to confirm high Mg concentrations. Following the above described procedure all dolostone grains previously untreated were repeatedly leached using the same strength leaching solution (0.005 M hydroxylamine hydrochloride as described above) for different periods of time and after each leaching step the supernatant was collected and treated the same way as all sediment samples. Leaching steps included a short leach for 60 s (SL), a long leach for 1 hr (LL), an overnight leach (NL) and the dissolution of the residual dolostone material after the previous three steps in 6 M nitric acid (RD) (Blaser et al., 2016; Huang et al., 2020). Due to limited sample size and very low Nd concentrations (<5 ppb) the Nd isotope compositions of the different leaching steps could not be measured for all samples.

The residual silicate digestion procedure of the detrital fraction was modified from Burton et al. (2002). Detailed description of the procedure could be found in Filippova (2016, PhD Thesis). Briefly, 100 mg of the previously leached sediment were leached for a second time for 6.5 hr, using the full strength leaching solution (Gutjahr et al., 2007) to completely remove any residual coatings or carbonates. Subsequently all samples were treated with a combination of concentrated nitric, hydrochloric and hydrofluoric acids. To dissolve all refractory minerals, including zircon, all samples were placed in metal jacket bombs in an oven at 200°C in a mixture of concentrated nitric and hydrofluoric acids for at least 4–5 days. After complete dissolution the samples were dried down, treated with perchloric acid to remove remaining organic matter, dried down again and re-dissolved in the loading solution for cation chromatography.

Neodymium isotope compositions of the foraminifera and dolostone grains were measured on a Thermo Finnigan Neptune Plus MC-ICP-MS, while measurements of Nd isotope ratios of the leachates and of residual silicate digests were carried out on a Nu Instruments MC-ICP-MS, both located at GEOMAR Helmholtz Centre for Ocean Research Kiel, Germany. All measured Nd isotope compositions were corrected for instrumental mass bias applying a $^{146}Nd/^{144}Nd = 0.7219$ using the mass bias correction procedure of Vance and Thirlwall (2002). All $^{143}Nd/^{144}Nd$ ratios were normalized to the accepted JNdi-1 standard value of 0.512115 (Tanaka et al., 2000). The external reproducibility of foraminifera data was assessed based on repeated measurements of an in house laboratory standard at a concentration of 10 ppb ($n = 14$) giving a 2 S.D. of 0.3 ε_{Nd}. The external reproducibility of the dolostone grain data was based on repeated measurements of a JNdi-1 standard solution with different concentrations of 5, 10, and 20 ppb Nd ($n = 15$) giving a 2 S.D. of 0.56, 0.3, and 0.2 ε_{Nd}, respectively. The external reproducibility of the leachate and residual silicate digests based on repeated measurements of JNdi-1 standard of different concentrations (150, 100, 60, and 50 ppb) on the Nu Instruments MC-ICP-MS varied between 0.2 and 0.5 ε_{Nd} units ($n = 7$ to 11 per session, 2 S.D.), with one exception where 2 S.D. was 0.8 ε_{Nd} units. The average long-term reproducibility for the Nu Instruments MC-ICP-MS was 0.4 ε_{Nd} units ($n = 95$, 2 S.D.) over the course of 3 years. The foraminifera blank was less than 89 pg and can be considered negligible. Blanks for leachates ($n = 6$) and the residual silicate digests ($n = 5$) were less than 38 and 1,270 pg, respectively and are negligible (less than 1% of the total amount of Nd in the samples).

A homogenized large volume sediment sample was used as an internal reference material and analyzed separately with every batch of samples. The reproducibility of the leachate measurements of this in house standard was 0.3 for ε_{Nd} (2 S.D., $n = 5$).

Concentrations of REE and major elements like Mg, Ca, Fe, Al (Table S4) were determined using ICP-MS (Agilent 7500ce). Concentration measurements of REE in the dolostone grains were carried out on a sample aliquot (~1/3 of the total sample volume) that had been separated prior to ion chromatography. Samples were dried down and redissolved and diluted in 2% HNO_3 with In or Re added as an internal standard. Dilutions of a commercial multiple REE standard solution from the Inorganic Ventures and a limestone reference material ECRM 752-1 were run with the samples for the calibration of signal intensities and quality control. The % of the 2 S.D. for ECRM 752-1 material was less than 1%. Average blank acid counts ($n = 10$) were subtracted from the raw sample counts. Concentrations below or close to three times the detection limit (3 S.D. of the blank) were not considered for interpretation.

3. Results

The down core authigenic Nd isotope compositions of the leachates in all 4 sediment cores follow similar trends as those of the residual silicate digest (Figures 2 and 3b). Good reproducibility of duplicate samples within the
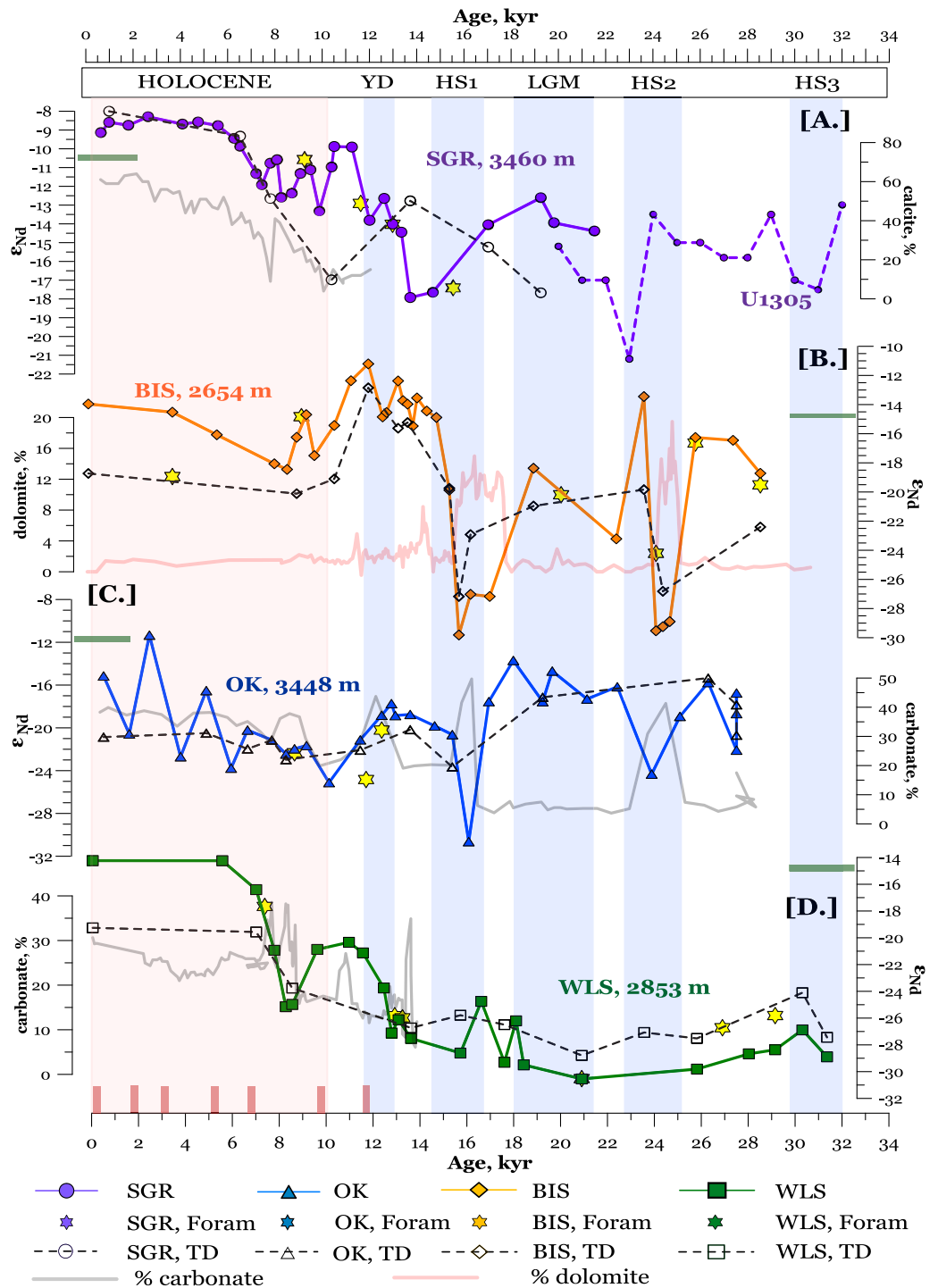
Figure 2. (a, b, c, d) The seawater ε_{Nd} signatures extracted from the ferromanganese coatings, uncleaned foraminifera and residual silicate digests (TD) of four sediment cores from this study. In the background light gray lines show the detrital carbonate content. data from (Hillaire-Marcel & de Vernal et al., 1989; Hillaire-Marcel et al.,1994; Fagel et al., 2004; Nuttin et al., 2015). In figure (a) The record is extended based on ε_{Nd} signatures of the leachates from U1305 (Blaser et al., 2020). Vertical bars denote intervals of major events: Heinrich Stadial 3 (HS3), Heinrich Stadial 2 (HS2), Last Glacial Maximum (LGM), Heinrich Stadial 1 (HS1), Younger Drays (YD), 8.2 ka event. The red vertical bar denotes Holocene. Error bars are smaller than the symbol size. Small red bars on the bottom of the plot show the appearance of ash layers in the sediments from Iceland and regions of North Atlantic (Haflidason et al., 1999). Horizontal dark green bars show modern day seawater signatures from close by locations (Lacan & Jeandel, 2005; Lambelet et al., 2016).
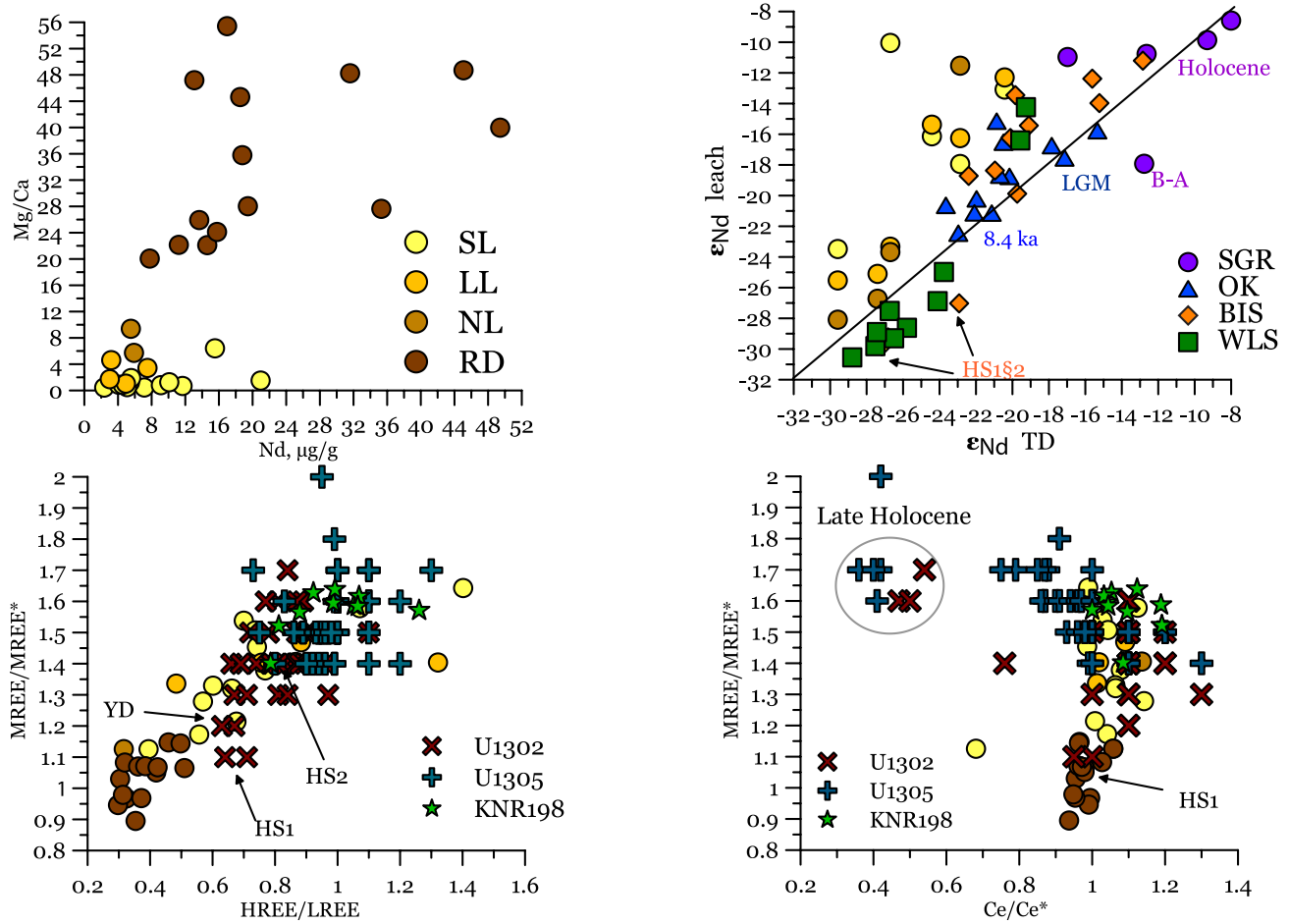
Figure 3. Dolostone grain leaching experiment results. SL stands for short leach (60 s), LL-long leach (1 hr), NL-over night leach, RD–residual dissolved dolostone grain. (a) Mg/Ca ratio of different dolostone leaching solutions versus Nd concentration in µg/g. (b) ε_{Nd} signatures of different dolostone leaching solutions versus totally dissolved residual dolostone (RD) together with ε_{Nd} signatures of the leachates from sediment cores from this study versus totally dissolved residual silicate data. (c) Rare Earth Elements (REE) ratios of the different leaching solutions of the dolostone grain and the totally dissolved RD from this study normalized to PAAS (McLennan, 2001), compared to REE ratios from cores U1302 and U1305 (Blaser et al., 2020). LREE, MREE, and HREE ratios were calculated using the following and normalized to PAAS (McLennan, 2001: LREE = La + Pr + Nd; MREE = Gd + Tb + Dy; HREE = Tm + Yb + Lu; MREE* = (LREE + HREE)/2 (Martin et al., 2010). (d) REE ratios versus Cerium anomaly of the different leaching solutions of the dolostone grain and the totally dissolved RD (residual dolostone (RD) from this study normalized to PAAS (McLennan, 2001), compared to REE ratios from cores U1302 and U1305 (Blaser et al., 2020).

uncertainties estimated by the precision obtained for an in-house reference material ($n = 0.5$, 2 S.D. = 0.3), large volume homogenized sediment sample that is run with every leaching batch suggests that the observed spatial and temporal variability seen in the leachate data over the last 32 kyr are not procedural artifacts or poorly homogenized sediment material, but due to nature of the processes dominating the signal formation in the Labrador sea and in the sediment column over the studied period of time. The ε_{Nd} signatures of the leachates range from −8.3 south of Greenland (∼2.6 ka, SGR) to −30.6 off the Orphan Knoll (∼16.4 ka, OK). A large but somewhat smaller range of variations is also observed in the residual silicate ε_{Nd} signatures within each core (overall −8.0, SGR to −28.8, WLS). Overall more radiogenic ε_{Nd} signatures of the leachates and detrital silicate fractions are recorded on the eastern part (SGR, Figure 2a) than in the western (Figures 2b and 2d) and southern parts of the Labrador Sea (Figure 2c).

During the LGM the sediment records from intermediate depths of the western Labrador Sea are generally less radiogenic than at the deeper cores with Nd isotope signatures of the leachates being ε_{Nd} ∼ −18 and −30.5, at BIS and WLS, respectively and residual silicate digests ranging between −21 and −28.8, at BIS and WLS respectively. In contrast, the deeper core ε_{Nd} signatures of the leachates (ε_{Nd} ∼ −14.5, SGR) and residual silicate digests (ε_{Nd} ∼ −17.4, OK) are more radiogenic. Highly unradiogenic values of both leachates and residual silicate fraction

in the WLS core on the Western Labrador slope persist from 32 ka until the YD. Highly unradiogenic excursions of up to 13 ε_{Nd} units observed in the leachate data during Heinrich stadials 3, 2 and 1 reaching ε_{Nd} signatures as low as −30.6 (∼16.4 ka, OK) are also reflected by negative ε_{Nd} shifts of the residual silicate digests of up to 7 ε_{Nd} units to ε_{Nd} signatures as low as −23.7 (OK, HS1). Interestingly, the Nd isotope signatures of the leachates at core BIS during HS1 and HS2 are even less radiogenic than those of the residual silicate digests. The time of the Bolling–Allerod warming is marked by a radiogenic ε_{Nd} excursion of the residual silicate digests of variable amplitude in all cores (Figure 2). The period between the end of the YD and the Early Holocene is characterized by an overall decrease in ε_{Nd} values of the leachates and residual silicate digests. Signatures akin to modern day DSOW (NWABW) and NEADW are recorded in the eastern Labrador Sea (leachates, SGR ∼ −9.9, BIS ∼ -11.2, Figures 2a and 2b) as early as 12 ka. The inception of the Holocene coincides with an unradiogenic excursion of about four ε_{Nd} units in BIS, SGR and OK cores. Overall, more radiogenic ε_{Nd} signatures of the leachates during the Holocene at all locations are only interrupted by a short dip around the time of the 8.2 ka event. The ε_{Nd} signatures of the residual silicate fraction are less variable with a trend toward more radiogenic values during the early Holocene and relatively constant values during the middle and late Holocene. The middle and late Holocene Orphan Knoll record exhibits high frequency variability of up to nine ε_{Nd} units in ε_{Nd} signatures of the leachates not seen in the detrital data, likely as a result of the lower resolution. The youngest leachate samples match modern day water mass signatures at the corresponding depths including DSOW south of Greenland and LSW in the western Labrador Sea (WLS, BIS, Figures 2bB and 2d). At the Orphan Knoll core (Figure 2c) the youngest targeted sedimentary depth (0.9 ka) is less radiogenic than ambient average DSOW (NWABW) published by Lambelet et al. (2016) from a close by location (OK ε_{Nd} ∼ −15.1 vs. −11.79, st. 9, 3,745 m). The ε_{Nd} signatures of the residual silicate digests of the uppermost samples of the WLS and BIS cores are 8–9 ε_{Nd} units more radiogenic than those of the residual silicate digests of the surface sediment samples from the western Labrador Slope (sample 3, ε_{Nd} ∼ −27.2, Figure 1, Table S2), whereas for the Orphan Knoll core the residual silicate ε_{Nd} signature of the uppermost sample of ∼ −20.9 is close to the range of surface sediment samples analyzed in this study (samples 2,4,5,6, Figure 1; ε_{Nd} between −22 and −26, Table S2). The core-top leachate ε_{Nd} signatures off the Orphan Knoll and off Iceland show better agreement with the modern seawater data from nearby stations (Lacan & Jeandel, 2005; Lambelet et al., 2016; Figure S1 in the Supporting Information S1), whereas more variability and offsets between bottom seawater and authigenic ε_{Nd} signatures are observed along the western Labrador shelf that could reflect the complex bathymetry of the region complicated by presence of numerous mounds in the area that can affect bottom current movement (Meredyk et al., 2020; Figure S1 in the Supporting Information S1).

The Mg/Ca ratios of dolostone leaching solutions range between 0.45 and 55 (Table S4), with the majority of samples in SL and LL steps falling between 0.45 and 1, characteristic for dolomite. The totally dissolved residual dolostone grains are more enriched in Mg, whereas the first three leaching solutions have significantly higher Ca concentrations (Figure 3a, Table S4). The Nd concentrations in dolostone grains range from 2 to 50 ppb, which is in agreement with previous analysis of dolostone material (Hecht et al., 1999; Kučera et al., 2009; Kuebler et al., 2020; Le Bas et al., 2007; Wang et al., 2017; Yang et al., 2009). The ε_{Nd} signatures of the residual digests of the dolostone grains (RD, 6M HNO_3) analyzed in this study have highly unradiogenic values that vary from −19.2 (SGR, 13.8 ka, Table S3) to up to −30 (OK, 9 ka, Figure 3b). The analysis of solutions extracted after short, long and overnight leaching of dolostone grains (SL, LL, NL) show two trends. On the western Labrador shelf (WLS and BIS) ε_{Nd} signatures of dolostone grains become more radiogenic with progressive leaching (SL, LL, NL), while the residual fraction of the dolostone digested in 6M HNO_3 (RD) shows the least radiogenic signatures and the highest Nd concentrations (Figures 3a and 3b). In core OK dolostone grains with each progressive leaching step (SL, LL, NL) become less radiogenic with the least radiogenic value for residual fraction (RD). Differences in detrital carbonate abundance between the Orphan Knoll sediments and other sites in the North Atlantic have been observed before (Hemming et al., 1998). This may suggest different source regions of the dolostone material. Highly unradiogenic water signatures reported by Grenier et al. (2022) for Canadian Arctic rivers draining areas with known dolostone formations (Brown et al., 2020; Dewing et al., 2007; Kah et al., 1999; Mathieu et al., 2013) may suggest the northern Baffin Island or Victoria Island as a potential source of dolostone with highly unradiogenic ε_{Nd} signatures for Orphan Knoll.

4. Discussion

Recent studies of radiogenic Nd isotopes have questioned their use as a deep water mass circulation and mixing proxy of the past and have shown that the authigenic ε_{Nd} signal can be altered due to exchange with pore waters

enriched with Nd from easily leachable minerals (volcanogenic material or detrital carbonates) preferentially dissolving in the sediment after deposition (Abbott et al., 2021; Blaser et al., 2016; Dausmann et al., 2019). Additionally, if the authigenic oxides and coatings do reflect a bottom seawater signature this can be affected by a strong pore water flux to the bottom waters (Abbott et al., 2019, 2021; Blaser et al., 2020; Pöppelmeier et al., 2022), and all processes related to the broader influence of boundary exchange on seawater Nd isotope signatures (e.g., Jeandel, 2016) superimposed on any influence of water mass mixing. Although some core-top samples along the western Labrador slope tend to have less radiogenic values than seawater from close by stations, the uppermost sediment samples from the BIS, WLS, and SGR cores as well as surface sediment samples off Iceland show good agreement with the modern day ε_{Nd} seawater signatures and range between modern LSW ($\varepsilon_{Nd} \sim -14.9$) (Lambelet et al., 2016; Figure S1 in the Supporting Information S1) and modern DSOW -10.5 (Lacan & Jeandel, 2005; Figure 2).The majority of the ε_{Nd} signatures obtained from the Fe-Mn coatings of leached sediments are in good agreement with ε_{Nd} signatures of uncleaned foraminifera (within uncertainties) from the nearest available depths in the sediment cores or consistent with the trends in the data with only a few exceptions (Figure 2).

The study area has been affected by repeated episodes of intensified iceberg-drift and meltwater inputs that resulted in the deposition of about 150 m thick braided sand abyssal plain and detrital carbonate layers as a result of ice sheet dynamics during the last 32 ka (Hesse & Khodabakhsh, 2006). In order to disentangle the effects of different conservative (only water mass mixing) and non-conservative (benthic flux, pore water exchange, diagenesis) processes on the recorded ε_{Nd} signals by Fe-Mn coatings of the sediments and chemically uncleaned foraminifera, we structure our discussion into three sections. First, we discuss the effect of high detrital carbonate deposition events on the bottom water signatures and evaluate the degree of potential pore water exchange in the sediment column during this time. In the second section we discuss the origin of ε_{Nd} signatures during the LGM, when detrital carbonate deposition associated with Heinrich stadials 1 and 2 ceased. The third section focuses on the nature of the Holocene variability of authigenic Nd isotope signatures.

4.1. The Origin of Radiogenic Nd Isotope Signatures in The Labrador Sea During High Carbonate Deposition Periods

Reoccurring high detrital carbonate deposition events have been recorded in Labrador Sea sediments over the course of the last 32 kyr. Distinct sediment layers containing high fractions of IRD and coarse fraction material as well as low abundances of foraminifera were primarily deposited in the Western North Atlantic during Heinrich Stadials (Heinrich, 1988). In the western Labrador Sea high detrital carbonate contents have also been observed during the Bolling-Allerød episode (BIS, WLS cores), the YD (OK) and during Early Holocene (WLS, OK) (Figures 2 and 4). In comparison to the North Atlantic, Heinrich layers in the Labrador Sea are much thicker ranging between 1 and 3.65 m versus 35 cm in the North Atlantic and contain markedly higher concentrations of detrital carbonate calcite and dolomite from dolostone in particular ($\approx$20%) (Hesse & Khodabakhsh, 2016). The detrital and authigenic ε_{Nd} signatures in all our records shifted toward highly unradiogenic values during these periods of time. On the western Labrador side a narrow range of signatures between -25 (OK) and -30 (WLS and BIS) was recorded during Heinrich events, whereas slightly more radiogenic signatures are seen off the southern tip of Greenland -22 (U1305, Figure 2). Marked peaks in coarse fraction and carbonate abundances during YD and B-A seen in cores PC13 (core located in close proximity to SGR), WLS and OK were followed by negative excursions in ε_{Nd} values, but to a lesser extent (Figure 4), possibly due to much lower dolomite abundance in the sediment based on the data from BIS core during B-A (Figure 4b). Carbonate-free clay size fraction data from Barber et al., 1997 from the western Labrador slope and Fagel et al. (2002) at the OK location show more radiogenic values during Heinrich stadial 1 and 2 ($\varepsilon_{Nd} < -28.7$) in comparison to our leachate data ($\varepsilon_{Nd} \sim -32$, Figure 4). Silt size fraction data (2–63 µm) from a location off the southern tip of Greenland (Innocent et al., 2000) also exhibit more radiogenic values at the time of Heinrich Stadial 2 ($\varepsilon_{Nd} \sim -19$). A gradual increase in detrital calcite content (dolomite close to zero) in the BIS core over the course of the Holocene (Figure 4b) is accompanied by radiogenic ε_{Nd} signatures of both the leachates and the detrital fraction (Nuttin et al., 2015). At the same time mineralogical abundance of different types of clay minerals at OK (Fagel et al., 1997) and BIS (Nuttin et al., 2015) core locations during Heinrich stadials 1 and 2 were significantly reduced, potentially due to increased supply of other IRD related material like very fine dolostone that is up to 80% contained in the very fine clay size fraction (Khodabakhsh, 1997).

Sequential leaching of dolostone grains picked from each sediment core reveals leaches (SL, LL) associated with Mg/Ca ratios close to 1 (Figure 3a) have unradiogenic ε_{Nd} signatures of down to -24 (Table S3). Even less
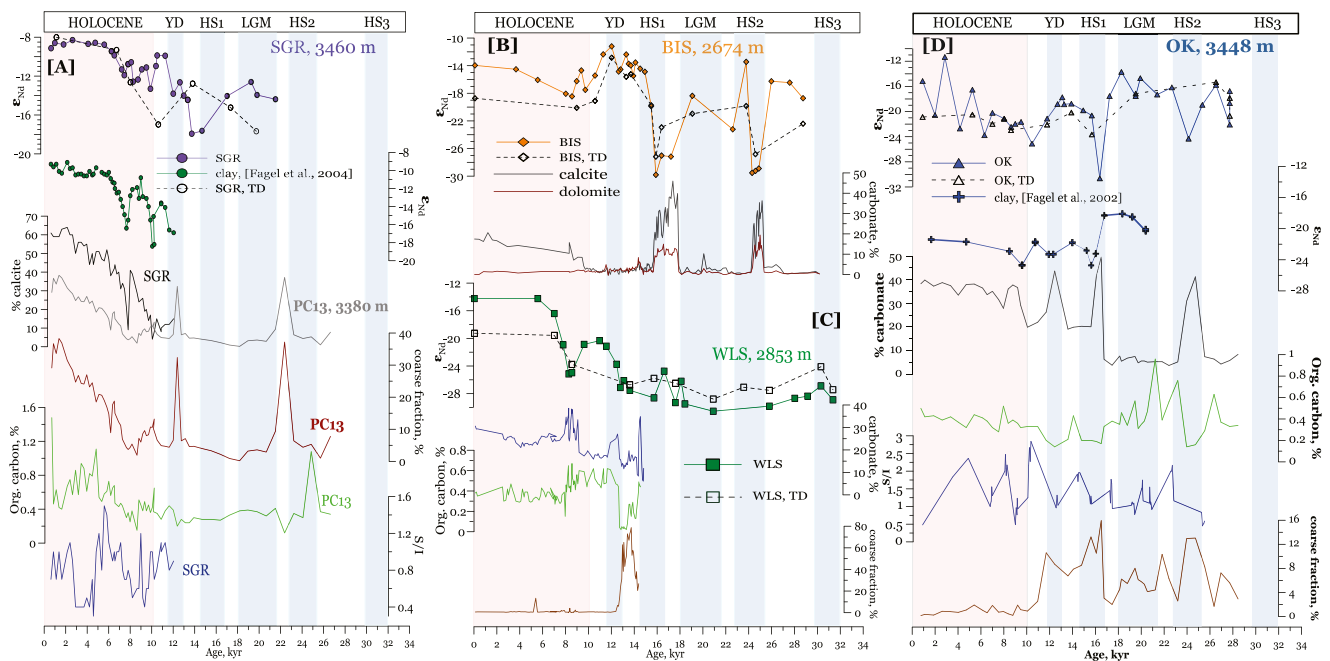
Figure 4. (a) Data from South Greenland Rise core (SGR) core. Top to bottom: The seawater ε_{Nd} signatures extracted from the ferromanganese coatings and residual silicate digests (TD); ε_{Nd} signatures of the detrital clay fraction (Fagel et al., 2004); % of detrital carbonate content from SGR core and nearby PC 13 (Fagel et al., 2004); % of coarse fraction PC13 (Fagel et al., 2002); % of organic carbon content PC13 (Fagel et al., 2002); smectite/illite ratio South Greenland Rise (Fagel et al., 1997) (b) Data from Baffin Island shelf core. Top to bottom: The seawater ε_{Nd} signatures extracted from the ferromanganese coatings and residual silicate digests; the carbonate content dolomite versus calcite in dw% (Nuttin et al., 2015) (c) Data from Western Labrador Slope core. Top to bottom: The seawater ε_{Nd} signatures extracted from the ferromanganese coatings and residual silicate digests; % of carbonate content (Hillaire-Marcel & de Vernal, 1989; Hillaire-Marcel et al., 1994); % of organic carbon content (Hillaire-Marcel & de Vernal, 1989; Hillaire-Marcel et al., 1994); the % distribution of coarse fraction (>125 μm) (Hillaire-Marcel & de Vernal, 1989; Hillaire-Marcel et al., 1994) (d) Data from OK core. Top to bottom: The seawater ε_{Nd} signatures extracted from the ferromanganese coatings and residual silicate digests; ε_{Nd} signatures of the detrital clay fraction (Innocent et al., 1997; Fagel et al., 2002); % of detrital carbonate content (Hillaire-Marcel & de Vernal, 1989; Hillaire-Marcel et al., 1994); % of organic carbon content (Hillaire-Marcel & de Vernal, 1989; Hillaire-Marcel et al., 1994); smectite/illite ratios (Fagel et al., 1997); % coarse fraction (Fagel et al., 1997).

radiogenic ε_{Nd} signatures of down to −30 are recorded in NL and RD leaching steps that also have the highest Mg concentrations (Figures 3a and 3b, Table S4). The Mg/Ca ratios and the Fe and Mn concentrations in SL and LL leaching steps of dolostone grains are within the concentration range presented by Kah et al. (1999), measured on samples from the Bylot Supergroup located in the northern part of Baffin Island, represented by successions of marine carbonate, including limestone and dolostone. Less radiogenic ε_{Nd} signatures of the NL and RD leaching solutions agree well with highly unradiogenic ε_{Nd} signatures of Canadian Arctic rivers that drain dolostone formations and post glacial sedimentary basins (Grenier et al., 2022). A study carried out by Andrews and Eberl (2011) also identified the northern Baffin Bay as a source of the dolomite that was carried along the southern Baffin Island shelf across Davis Strait into the Labrador Sea. Dolostones in this area are mainly referred to as hydrothermal dolostones formed via a complex process of early fluid circulation. Chemical characteristics of the circulating fluid are not limited to a specific geological period but to a specific tectonic environment (Lavoie et al., 2011). It is possible that detrital carbonates carry highly unradiogenic signatures of the surrounding geological settings like the Churchill or Superior Province with ε_{Nd} signatures $\geq$−30 given that the dolostone contains inclusions of minerals other than dolomite (Cousens et al., 2004; Sandeman et al., 2004, 2006). Recent studies on Canadian Arctic river waters also showed that they are more corrosive and undersaturated with respect to calcite (log Ω_{cal} up to −5, Alkire et al., 2017). This suggests that the partial dissolution of dolostone grains such as these are a potentially important source of highly unradiogenic Nd. Authigenic REE data from sediment cores U1305 (3,459 m) and U1302 (3,556 m, Blaser et al., 2020), located in close proximity to cores SGR and OK, respectively, plot together with the residual dolostone fraction (RD) for the section corresponding to Heinrich stadial 1 and the YD in U1302 (Figure 3c). The rest of the samples plot in the area of the Ca-rich portion of the detrital grains and have more radiogenic ε_{Nd} signatures. This further suggests that dissolution of detrital dolostone and associated preformed Fe-Mn oxide coatings affected the ε_{Nd} signatures during high detrital

carbonate deposition events. The pronounced return toward more radiogenic signatures after the cessation of detrital carbonate deposition less than 500 years later and the overall systematically unradiogenic ε_{Nd} signature during Heinrich stadials ($\varepsilon_{Nd} \sim -30$) and the YD in the Labrador Sea point to an influence of detrital dolostone dissolution across the entire basin. Below we propose potential mechanisms responsible for these observations together with an estimate of the degree to which dolostone dissolution may have affected the ε_{Nd} signatures of the authigenic fraction of Labrador Sea sediments.

4.1.1. Dissolution of Fine Dolostone Particles Sinking Through the Water Column

Dissolution of dolostone flour would only have occurred if bottom waters in the Labrador Sea were corrosive enough during Heinrich stadials. Records of calcite saturation state in nearby Baffin Bay water masses suggest the presence of dense calcite undersaturated waters, pulses of which entering the Labrador Sea through the Davis Strait, may have facilitated dolostone dissolution (Codling, 2017). Marshall et al. (2021) found only subtle evidence of dissolution at the BIS location during Heinrich stadial 1 due to low sample resolution, however, the authors did not exclude the possibility of intense dissolution caused by an increased terrestrial organic carbon flux (Gibb et al., 2014). Enhanced carbonate dissolution during Heinrich Stadials in the Labrador Sea and the North Atlantic is also supported by model studies forced by the fresh water inflow in the North Atlantic region that suggest significant decrease in carbonate burial flux (Chikamoto et al., 2008). Studies by Ezat et al. (2017) and Yu et al. (2019) show lower carbonate ion concentrations during Heinrich events in the Nordic Seas, suggesting more corrosive water conditions. Present day studies of the Gulf of St. Lawrence catchment have revealed the importance of dolomite weathering and dissolution in the region for the overall HCO_3^- runoff budget (Szramek et al., 2007). In addition, studies from the modern day Canadian Artic (south and east of Victoria Island) show that these waters are more corrosive due to undersaturation with respect to calcite (log Ω_{cal} between -3.01 and -5.09, Alkire et al., 2017), lower alkalinity and dissolved carbonate ion concentrations (Chierici & Fransson, 2009; Grenier et al., 2022). The opposing temperature dependence of calcite and dolomite dissolution rates results in progressively greater dolomite solubility under temperatures below 25°C relative to that of calcite (Drever, 1997; Langmuir, 1997). This potentially played a significant role in detrital carbonate dissolution during meltwater flood events. Also the addition of large volume of fresh waters to the Labrador basin (Table S5) could have lowered the saturation state of the basin, similar to the situation observed in the modern day Canadian Arctic waters affected either by river runoff or sea ice meltwater input (Chierici & Fransson, 2009). The above arguments suggest that it is not unlikely that during Heinrich stadials conditions in the Labrador Sea could have been favorable for detrital carbonate dissolution.

Previously various sources have proposed to explain the observed unradiogenic ε_{Nd} excursions seen in marine sediment records during Heinrich events. Roberts and Piotrowski (2015) suggested that IRD material sinking through the water column could have resulted in the "re-labeling" of the seawater Nd isotope composition, which was subsequently recorded by coatings of foraminifera. Howe, Piotrowski, and Rennie (2016) proposed a more "bottom up" source, suggesting that poorly chemically weathered detrital material deposited at the bottom of the Labrador Sea could have been the source of highly unradiogenic Nd at abyssal depths. The latter assumption is consistent with highly unradiogenic signatures of the authigenic fraction of Heinrich stadial sediments with the unradiogenic signatures carried by the residual part of the dolostone grains. Study by Hesse and Khodabakhsh (2016) described in detail the potential mechanism, how this detrital material was delivered to the bottom of the Labrador Sea. During the movement of a turbidity current a cloud of lofted fine sediments forms from the particles that rise up from the main body of the current. Sand loaded turbidity currents generated by melt water discharge at ice sheet margins have a very high particle density (Hesse et al., 2004) that allows them to overcome seawater density barriers, resulting in a cloud of fine grain-sized sediments that can rise up to 1–3.5 km water depth (Hesse & Khodabakhsh, 2006). Following the level of equal density in the stratified water column, such a sediment cloud could then spread horizontally, depositing fine grained silt and clay along its way. This mechanism is likely responsible for the deposition of tens of individual stacked graded sediment mud layers with thicknesses from millimeters to centimeters that contain IRD observed within a 300 km distance to the Hudson Strait ice stream outlet (Hesse & Khodabakhsh, 2006, 2016). The deposition of these sediments may have taken anywhere from a few days up to a decade based on particle size settling times (See Text S1.1 in the Supporting Information S1). The efficient grinding of Paleozoic carbonates by LIS glaciers produced glacial flour containing fine detrital carbonate susceptible to dissolution while sinking through the water column. First order calculations of particle load based on sediment mud layer thickness and total sediment release, yield sediment loads on the order of 3.7 mg/L (0.2 cm) to 56.2 mg/L (3 cm) depending on the thickness of the mud layers. This corresponds to

between 31×10^{10} kg and 472×10^{10} kg of fine grain sized sediments deposited per individual mud layer with an average dolomite content of about 20% (See Text S1.2 in the Supporting Information S1, Nuttin et al., 2015). This is consistent with other studies that estimated the total sediment release including all mud layers and total glacial IRD flux during Heinrich stadials to be on the order of 1×10^{15} kg (Alley & MacAyeal, 1994; Hemming, 2004; Hesse & Khodabakhsh, 2016; Roberts et al., 2014; Table S5). Based on the estimated dissolution rate of dolomite minerals between 0.3 and 4.5×10^{-4} mmol/kgH$_2$O yr^{-1} (Deike, 1990), only a fraction of this dolomite in dolostone could be dissolved. In the case of lower dissolution rate and lower Nd concentrations considered (7 µg/g, Table S4), the amount of released Nd per liter of water (9.68 pg/kgH$_2$O) would not be sufficient to shift the ε_{Nd} signatures of the bottom water to highly unradiogenic values as recorded at our sites. Higher dissolution rates and Nd concentrations (49 µg/g), however, account for 1,016.5 pg/kgH$_2$O of Nd released into the water column. This would be enough to shift the ε_{Nd} signatures of bottom waters to -30, which is consistent with the recorded signatures in cores WLS and BIS that are located within a 300 km distance from the mouth of the Hudson Strait ice stream. Analysis of the grain size distribution by Hesse and Khodabakhsh (2016) showed that about 15% of the sediment in these mud layers are represented by a very fine fraction that could take up to 13 years to settle (See Text S1.1 in the Supporting Information S1). A longer settling time in comparison to the coarser fraction can result in higher Nd release from the fine fractions resulting in Nd concentrations from 0.5 ng/kgH$_2$O up to 52.8 ng/kgH$_2$O in the bottom 1 km of the water column (Text S1.3 in the Supporting Information S1). In a simple two end-member mixing model admixture of between 90% (OK) and 40% (SGR) of this water mass along the flow path would be enough to shift the ε_{Nd} signatures to the observed unradiogenic values in the case of a 0.5 ng/kgH$_2$O concentration shift (Figure S2 in the Supporting Information S1). This suggests that the dissolution of dolomite contained in dolostone or other mineral inclusions associated with dolostone flour may plausibly have been the sole source of the observed negative ε_{Nd} signatures across the Labrador Sea during Heinrich stadials, even without invoking a benthic flux or pore water exchange.

4.1.2. Benthic Nd Flux From Dolostone Deposition and Release

Deposition of dolostone material and subsequent partial dissolution and release may have been another important source of Nd in the bottom waters of the Labrador Sea. Oxidation of reworked terrestrial organic material combined with sediment supply during outburst floods may have resulted in increased acidity of the uppermost sediment layer, promoting dissolution of dolostone and its release into the bottom water. First order estimations suggest that the benthic flux was on the order of 40 pg [Nd]/cm^2 yr^{-1} to 4 ng [Nd]/cm^2 yr^{-1} of Nd depending on the dissolution rate and Nd concentration of the dolomite (see Text S2 in the Supporting Information S1). These estimations are in the same range as fluxes proposed by Abbott et al. (2015) and Blaser et al. (2019) for the Heinrich layers. An accurate estimation of how much dolostone was exposed to bottom water interaction is, however, difficult due to the inhomogeneous distribution of the grains in the sediment layers. However, first order calculations of the detrital carbonate sourced benthic Nd flux suggest that it had a significant effect at least locally in areas (WLS, BIS) where these mud layers containing a high percentage of fine-grained dolostone occurred. The actual benthic Nd flux originating from dolostone dissolution into the bottom waters at the OK and SGR core locations was most likely at the lower end of this range. At these locations different mechanisms of sediment deposition during Heinrich stadials like turbidity current-driven spillovers would have reduced both the amount of the dolostone exposed to bottom water and the overall time of exposure (Hesse & Khodabakhsh, 2016).

4.1.3. Dolostone (Dolomite) Dissolution in Pore Waters Post Deposition

The dissolution of detrital material enhancing pore water Nd concentrations has been discussed extensively in many studies of authigenic Nd signatures (e.g., Elderfield & Sholkovitz, 1987; Haley et al., 2004). The alteration of authigenic signatures after deposition via exchange with sedimentary pore waters has been proposed before by Abbott et al. (2019, 2021) and others, and has been estimated by Blaser et al. (2020) for the Labrador Sea sediments based on data on authigenic and detrital REE concentrations from nearby core sites. Rare earth element patterns normalized to shale provide additional information on the processes that take place within the sediment column, where MREE bulge pattern has been attributed to the Fe- and Mn reduction processes and MREE release in pore waters, HREE enrichment to respiration processes and flatter patterns are attributed to sulfate reduction (Smrzka et al., 2019). REE patterns of residual dolostone grains (RD) either exhibit a slightly negative Ce anomaly to no anomaly, and a relative LREE enrichment (Figure S2 in the Supporting Information S1). More Ca-rich leachates of the grains show a MREE bulge and LREE depletion (SL) (Figure S2 in the Supporting Information S1), which have also been observed by Blaser et al. (2019) in the REE patterns from the Heinrich

stadial intervals and leached IRD samples. Comparison of REE data from dolostone leaching experiment with REE data available from Blaser et al. (2020) shows that core Site U1302 has lower MREE/MREE$^\times$ values and lower Ce/Ce$^\times$ during Heinrich stadials (Figures 3c and 3d), similar to the residual dolostone fraction, suggesting some pore water dissolution. Unradiogenic signatures during Heinrich stadials at the locations of both Sites U1302 and U1305 also corresponded to an increase in Mg concentration of bulk sediments (Blaser et al., 2020). This suggests that dolostone dissolution may have influenced the ε_{Nd} signatures at our locations due to the very close proximity to our cores. However, our data show sharp changes of ε_{Nd} signatures of up to 10 ε_{Nd} units over 10–20 cm intervals that are confined to the sections showing high detrital dolostone content, which suggests no Nd diffusion out of the Heinrich layers (Figure 2). However, in the case of dolostone dissolution it is not possible at this point to unambiguously state if the leached sediment fractions acquired those unradiogenic signatures from pore waters or through dolostone dissolution at the seawater-sediment interface and thus reflect relabeled bottom water signatures. In addition, the Mg rich residual dolostone (RD) has high Nd concentrations (between 7 and 49 µg/g) and lower MREE concentrations, whereas the Ca rich fraction of the detrital dolostone grains has generally lower Nd concentrations (2–20 µg/g) and more MREE enrichment. Blaser et al. (2020) observed no obvious change in Nd concentration during Heinrich Stadials at Site U1302 and U1305 locations.

The single mixed foraminifera coating value (−24.2) from the Heinrich stadial 1 (BIS) has an ε_{Nd} value that is about 5 ε_{Nd} units more radiogenic than the leachate and agrees well with the range of ε_{Nd} signatures associated with dissolution of dolomite portion of dolostone grains (ε_{Nd} between −15 and −24, SL, NL, LL steps, Table S3). This suggests that even if during leaching a more reactive phase was attacked, its effect only partially contributed to the observed unradiogenic signatures recorded during Heinrich stadials and unradiogenic signatures <−24 reflect the effect of dolomite dissolution in the water or sediment column. The unradiogenic excursion at SGR location distant from the source of the detrital carbonates during Heinrich Stadial 1 in uncleaned foraminifera (ε_{Nd} ~ −18) is in agreement with a water mass mixing signal. Overall reduced presence of detrital carbonate in this core ≤5% in comparison to 20%–40% in other cores suggests that the dolostone contribution to pore waters was minimal.

Consistently highly unradiogenic ε_{Nd} signatures of ~−30 of the leachates and of uncleaned foraminifera (Figure 2) at the WLS location for the period between 32 ka and the YD that are less radiogenic than the residual silicate fraction suggest that at this location authigenic signatures may have been overprinted after deposition due to dissolution of dolostone associated reactive mineral phases and Nd release into pore waters. An alternative explanation could be advection of highly unradiogenic water with the LC from the Baffin Bay. Coarse fraction data (≥125 µm, ~20%) and very low δ^{18}O signatures indicate continuous supply of meltwater from the Labrador Sea margin to the location that most likely was confined to the shelf break (Hillaire-Marcel & de Vernal, 1989; Hillaire-Marcel et al., 1994). Cold temperatures and brine rejection may have made the glacial analog of the Labrador current denser, thereby facilitating its penetration to deeper layers. Highly unradiogenic signatures may have been set through similar processes of detrital carbonate (dolostone) dissolution in the Baffin Bay water column. Previous studies have shown that Baffin Bay sediments have even higher dolomite content (≥30–40%) than those of the Labrador Sea (Jackson et al., 2017; Simon et al., 2014) and unpublished detrital and authigenic ε_{Nd} data from Baffin Bay sediments suggest highly unradiogenic values around this time (Kirillova, 2017).

Unradiogenic values recorded in uncleaned foraminifera at OK (ε_{Nd} ~ −25) during the YD at the time of detrital carbonate increase are similar to those of the residual dolostone (ε_{Nd} ~ −26.7, Figure 5) picked from the YD interval, suggesting that dolostone dissolution affected the signatures. However, unradiogenic excursions are also recorded south of Greenland at U1302 (ε_{Nd} ~ −23), SGR and U1305 (ε_{Nd} ~ −13.4) and PC13 (ε_{Nd} ~ −16.7) locations, and although the dolomite dissolution to various degree could not be completely ruled out, we suggest that this signal could have also been transported within the water masses. If the signatures were acquired post-depositionally at Orphan Knoll, we would not expect to see a gradient consistent with water mass mixing south of Greenland. In addition, carbonate abundance data from core SGR and U1305 show no change in detrital carbonate deposition (Figure 5). Increases in carbonate and coarse fraction abundances recorded in core PC13 at the same time most likely were the result of erosion of the eastern Greenland ice sheet and an intensified IC (Dyke et al., 2014; Jennings et al., 2006; Oksman et al., 2017; Rainsley et al., 2018; Seidenkrantz et al., 2021).

Based on the results of dolostone leaching experiment and the following above discussion we conclude that unradiogenic signatures recorded in the Labrador Sea during Heinrich stadials and the YD were set by dissolution of dolomite and other dolostone associated mineral phases. The presence of unradiogenic excursions across
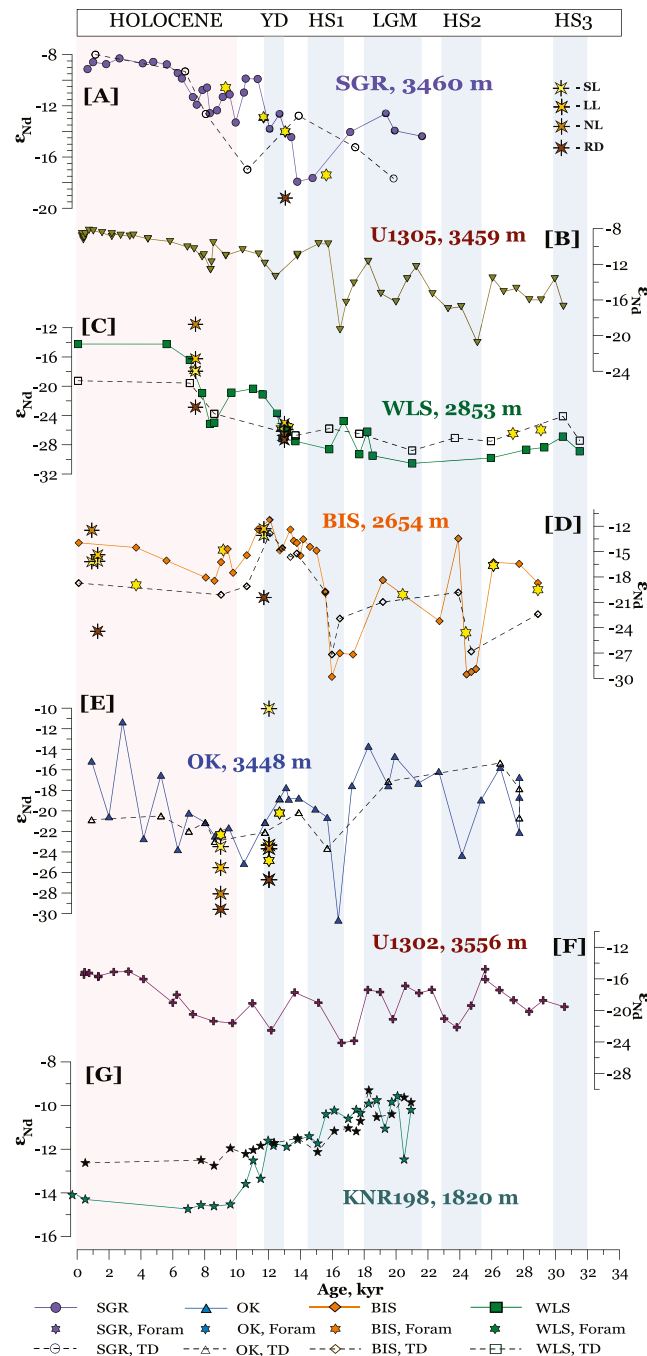
Figure 5. (a) The South Greenland Rise core seawater ε_{Nd} signatures extracted from the ferromanganese coatings, uncleaned foraminifera, residual silicate digests (TD) and dolomite leaching experiment. (b) Core U1305 (Blaser et al., 2020) seawater ε_{Nd} signatures extracted from the ferromanganese coatings (c) The Western Labrador Slope core seawater ε_{Nd} signatures extracted from the ferromanganese coatings, uncleaned foraminifera, residual silicate digests and dolomite leaching experiment. (d) The Baffin Island shelf core seawater ε_{Nd} signatures extracted from the ferromanganese coatings, uncleaned foraminifera, residual silicate digests and dolomite leaching experiment. (e) The OK core seawater ε_{Nd} signatures extracted from the ferromanganese coatings, uncleaned foraminifera, residual silicate digests and dolomite leaching experiment. (f) Core U1302 (Blaser et al., 2020) seawater ε_{Nd} signatures extracted from the ferromanganese coatings. (g) Core KNR198 (Zhao et al., 2019) seawater ε_{Nd} signatures extracted from the ferromanganese coatings. Error bars are smaller than the symbol size.

the Labrador Sea is in agreement with the advection of a water mass signal southward to Orphan Knoll and the southern tip of Greenland, suggesting that dolostone dissolution affected the water column signatures through dissolution in the water column or near the sediment water interface rather than contributions from pore waters.

4.2. Origin of the ε_{Nd} Signatures During the LGM

The end of the high detrital carbonate deposition event associated with Heinrich stadial two is marked by a radiogenic excursion of the authigenic ε_{Nd} signature in all cores, except WLS. LGM ε_{Nd} signatures in authigenic phases of Labrador Sea sediments recorded a remarkably narrow range of values between −13.9 (SGR) and −14.7 (OK, Figure 2). These signatures are in agreement with MREE corrected values for the LGM period (−15.8 ± 1.6), proposed by Blaser et al. (2020). The ε_{Nd} signature extracted from intermediate depth BIS core shows less radiogenic value of around −18.4 (Figure 2). Less radiogenic values and close proximity of the core to the Hudson Strait Ice Stream outlet suggest overprinting of the signature via partial dissolution of silicates or detrital clays. Dolomite content during this time was close to zero and the abundance of coarse fraction material was greatly reduced suggesting limited supply of detrital carbonates during this time period (Figure 4). LGM ε_{Nd} signatures of the leachates are only three ε_{Nd} units more radiogenic than the totally dissolved residual silicate suggesting extensive pore water exchange with the detrital silicates or clay fraction after deposition. This is consistent with recent modeling results suggesting an insensitivity of the authigenic Nd isotope signatures to the water mass structure in the North Atlantic as a function of an overall more sluggish deep water circulation and thus enhanced exchange with the sediments during the LGM (Pöppelmeier et al., 2022). Several lines of evidence nevertheless suggest the presence of an active deep ocean circulation in the Labrador Sea during the LGM. Seidenkrantz et al. (2021) found evidence of a strong boundary current activity and extensive influx of warm Atlantic source water, resulting in a stronger SPG and transfer of waters into the subpolar region and Labrador Sea. This is supported by an increase in smectite to illite ratio in the OK and BIS cores and the presence of clay minerals (smectite, kaolinite/chlorite) and of pyroxene only detected between 24 and 18 ka in BIS core (Nuttin et al., 2015). Studies by Simon (2012) and Simon et al. (2014) show an increase in smectite abundance in the sediments of the central Baffin Bay prior to the LGM followed by an increase in clay and silt fractions. An increase in smectite abundance can be explained by intensified erosion of Tertiary basalts of the North Atlantic Igneous Province (Figure 1), supported by the increased presence of pyroxene during this interval (Nuttin et al., 2015). The inflow of warm Atlantic water may have resulted in an early deglaciation of the western Greenland shelf and its intensified erosion delivering clay minerals and pyroxene into the Baffin Bay and subsequently the Labrador Sea (Dyke et al., 2014; Jennings et al., 2006; Oksman et al., 2017; Rainsley et al., 2018; Seidenkrantz et al., 2021). Data from Baffin Bay sediments of core SL174 (ε_{Nd} ~ −28.1, 20 ka, Kirillova, 2017) indicate highly unradiogenic signatures during the LGM. The position of the core on the Baffin Island side and within the path of the Baffin Island current thus allowed recording water mass transport to our core locations. As the Labrador Sea was surrounded by extensive ice sheets, enhanced shelf brine water production (Thornalley et al., 2015) likely played an important role facilitating the subduction of unradiogenic waters into deeper layers of the Labrador Sea along the western Labrador slope, providing the source of unradiogenic ε_{Nd} signatures further down the flow path.

4.3. Holocene

The Holocene period has been characterized by overall more radiogenic ε_{Nd} signatures, consistent with the inception of DSOW advection and the opening of Bering Strait. A large variability has nevertheless been recorded in our cores during the Early Holocene. An unradiogenic excursion recorded in all cores around 8.5 ka is consistent with a Hudson Bay Ice Saddle collapse that resulted in the freshening of the Labrador shelf water down to 200 m (Lochte, Repschläger, Kienast, et al., 2019). Data show no increase in coarse fraction abundance in the sediments on the western Labrador side. Although an increase in detrital carbonate abundance is observed, data from the BIS location show no presence of detrital dolomite. This suggest that the unradiogenic ε_{Nd} signatures recorded around 8.5 ka unlikely resulted from deposition of poorly chemically weathered sediments to the Labrador Sea basin as proposed by Howe, Piotrowski, and Rennie (2016). At the SGR the clay size fraction shows an unradiogenic excursion (Figure 4a) that is not associated with an increase in abundance of different types of clay minerals (Fagel et al., 2004), while leachate data show the opposite trend suggesting that dissolution of clay size in pore waters is also an unlikely source. However, Lake Agassiz and Keewatin ice dome were draining the area of Canadian Arctic, characterized by highly unradiogenic river

water ε_{Nd} values during the modern day (Grenier et al., 2022). This suggest that it is possible that meltwater input signal carried highly unradiogenic Nd signatures and was advected around the Labrador Sea as a part of the Labrador current.

Repeated unradiogenic ε_{Nd} excursions observed in the record of the Orphan Knoll over the middle to late Holocene are not reflected by variations of residual silicate digest signatures, potentially due to their lower resolution. Repeated fluctuations in the S/I ratio at OK and SGR records over this period, together with small changes in % of carbonate abundance content in OK core (Figures 2 and 4) suggest changes in the position of the LC and NAC relative to the site locations. This is supported by the short-term unradiogenic excursions detected around 6.5, 4.4, and 2.2 ka in the OK record (Figure 2) followed by cold spells recorded in Mg/Ca data from Reykjanes Ridge around these times (Moros et al., 2012). A drastic decrease in S/I ratios at the OK location after 5 ka and less radiogenic detrital signatures on the western Labrador slope over the Holocene suggest an increased influence of the Labrador current delivering unradiogenic sediments to the Orphan Knoll, indicating the establishment of the modern-day circulation in the Labrador Sea. Deep water formation in the Labrador Sea reached up to 2600 m depth during the middle and late Holocene off the Baffin Island Strait and in the western Labrador Sea, suggesting a stronger than present day convection in the region. This is plausible given that prior to 1994 during the cold state of the Labrador Sea, LSW was detected at depths of up to 2,400 m (Yashayaev & Clark, 2006; Yashayaev & Loder, 2009). This is also supported by studies suggesting an increasingly colder and fresher WGC during the late Holocene (Moros, 2006; Perner et al., 2012), which may have promoted convection in the upper Labrador Sea due to reduced salinity gradients.

5. Conclusions

Over the course of the last 32 kyrs, the Labrador Sea experienced multiple detrital carbonate deposition events accompanied by high abundances of IRD and coarse fraction material and low abundances of foraminifera. We suggest that the highly unradiogenic ε_{Nd} signatures recorded during these periods in all records have at least partly been the result of dolostone associated mineral dissolution facilitated by favorable low temperatures and the presence of more corrosive fresh cold Arctic waters. First order estimations based on Nd concentration and Nd isotope signatures of dolomite grains suggest that dolostone dissolution in the water column or in the pore waters of the sediments subsequently released as a benthic flux would have been sufficient to cause the observed shifts. Although there are some signs of dolostone dissolution in pore waters, at least part of highly unradiogenic signatures were set in the water column and advected southwards. During the LGM generally more radiogenic signatures ε_{Nd} between −14 and −18 were recorded in comparison to high carbonate deposition events possibly indicating active water mass advection and mixing in the Labrador Sea rather than pore water exchange. The large ε_{Nd} variability during the Holocene indicates changes in the locations of LC and NAC flow supported by smectite to illite ratios. The ε_{Nd} signatures of core top samples suggest a significantly deeper water mass convection in the Labrador Sea down to 2,600 m.

The authigenic Nd isotope signatures in the Labrador Sea have clearly been affected by exchange processes with the sediments. Therefore, the environmental and depositional settings need to be comprehensively assessed to be able to apply radiogenic isotopes as a proxy that sheds light on the formation of past water mass end-member signatures, changes in weathering regimes or conditions that result in extreme signatures like the ones observed during Heinrich stadials. The climatically driven pulses of detrital carbonate depositions that accompanied or followed high volume melt water inputs have likely exerted an important control on the Nd isotope composition of authigenic phases and potentially even water masses in the Labrador Sea and need to be taken into account when reconstructing past changes.

Data Availability Statement

All the data are available in Table S1–S5 in the Supporting Information S1. All the data are available via PANGAEA (Filippova et al., 2022). The details of the calculations are described in the Supporting Information calculation file.

References

Abbott, A. N., Haley, B. A., & McManus, J. (2015). Bottoms up: Sedimentary control of the deep North Pacific Ocean's ε_{Nd} signature. *Geology*, *43*(11), 1035–1035. https://doi.org/10.1130/G37114.1

Abbott, A. N., Löhr, S., & Trethewy, M. (2019). Are clay minerals the primary control on the oceanic rare Earth element budget? *Frontiers in Marine Science*, *6*, 504. https://doi.org/10.3389/fmars.2019.00504

Abbott, A. N., Löhr, S. C., Payne, A., Kumar, H., & Du, J. (2021). Widespread lithogenic control of marine authigenic neodymium isotope records? Implications for paleoceanographic reconstructions. *Geochimica et Cosmochimica Acta*.

Alkire, M. B., Jacobson, A. D., Lehn, G. O., Macdonald, R. W., & Rossi, M. W. (2017). On the geochemical heterogeneity of rivers draining into the straits and channels of the canadian arctic archipelago. *Journal of Geophysical Research: Biogeosciences*, *122*, 2527–2547. https://doi.org/10.1002/2016jg003723

Alley, R. B., & MacAyeal, D. R. (1994). Ice-rafted debris associated with binge/purge oscillations of the laurentide ice sheet. *Paleoceanography*, *9*(4), 503e511. https://doi.org/10.1029/94pa01008

Andrews, J. T., Barber, D. C., Jennings, A. E., Eberl, D. D., MacLean, B., Kirby, M. E., & Stoner, J. S. (2012). Varying sediment sources (Hudson Strait, Cumberland sound, Baffin Bay) to the NW Labrador Sea slope between and during heinrich events 0 to 4. *Journal of Quaternary Science*, *27*, 475–484. https://doi.org/10.1002/jqs.2535

Andrews, J. T., Bond, B., Jennings, A. E., Kerwin, M., Kirby, M., Manley, W., et al. (1995). A heinrich-like event, H-0 (DC-0): Source(s) for detrital carbonate in the North Atlantic during the younger dryas chronozone. *Paleoceanography*, *10*, 943–952. https://doi.org/10.1029/95pa01426

Andrews, J. T., & Eberl, D. D. (2011). Surface (sea floor) and near-surface (box cores) sediment mineralogy in Baffin Bay as a key to sediment provenance and ice sheet variations. *Canadian Journal of Earth Sciences*. https://doi.org/10.1139/e11-021

Andrews, J. T., Keigwin, L., Hall, F., & Jennings, A. E. (1999). Abrupt deglaciation events and Holocene palaeoceanography from high-resolution cores, Cartwright saddle, Labrador shelf, Canada. *Journal of Quaternary Science*, *14*, 383–397. https://doi.org/10.1002/(sici)1099-1417(199908)14:5<383::aid-jqs464>3.0.co;2-j

Andrews, J. T., & Tedesco, K. (1992). Detrital carbonate-rich sediments, northwestern Labrador sea: Implications for ice sheet dynamics and iceberg rafting (Heinrich) events in the North Atlantic. *Geology*, *20*, 1087–1090. https://doi.org/10.1130/0091-7613(1992)020<1087:dcrsnl>2.3.co;2

Balsam, W. L., & Heusser, L. E. (1976). Direct correlation of sea surface paleotemperatures, deep circulation, and terrestrial paleoclimates: Foraminiferal and palynological evidence from two cores off Chesapeake Bay. *Marine Geology*, *21*, 121–147. https://doi.org/10.1016/0025-3227(76)90053-0

Barber, D. C., Farmer, G. L., & Andrews, J. T. (1997). Ice-flow paths during Heinrich events in the Hudson Strait region: Provenance data from Nd and Pb isotopes. *Eos Transactions, American Geophysical Union*, *78*, 311.

Bilodeau, G., Vernal, A. D., & Hillaire-Marcel, C. (1994). Benthic foraminiferal assemblages in Labrador Sea sediments: Relations with deep-water mass changes since deglaciation. *Canadian Journal of Earth Sciences*, *31*, 128–138. https://doi.org/10.1139/e94-011

Blaser, P., Gutjahr, M., Pöppelmeier, F., Frank, M., Kaboth-Bahr, S., Frank, N., & Lippold, J. (2020). Labrador Sea bottom water provenance and REE exchange over the past 35,000 years. *Earth and Planetary Science Letters*, *542*, 116299. https://doi.org/10.1016/j.epsl.2020.116299

Blaser, P., Lippold, J., Gutjahr, M., Frank, N., Link, J. M., & Frank, M. (2016). Extracting foraminiferal seawater Nd isotope signatures from bulk deep sea sediment by chemical leaching. *Chemical Geology*, *439*, 189–204. https://doi.org/10.1016/j.chemgeo.2016.06.024

Blaser, P., Pöppelmeier, F., Schulz, H., Gutjahr, M., Frank, M., Heinrich, H., et al., (2019). The resilience and sensitivity of Northeast Atlantic deep water εNd to overprinting by detrital fluxes over the past 30,000 years. *Geochimica et Cosmochimica Acta*, *245*, 79–97. https://doi.org/10.1016/j.gca.2018.10.018

Böhm, E., Lippold, J., Gutjahr, M., Frank, M., Blaser, P., Antz, B., et al. (2015). Strong and deep Atlantic meridional overturning circulation during the last glacial cycle. *Nature*, *517*, 73–76.

Bond, G., Heinrich, H., Broecker, W., Labeyrie, L., Mcmanus, J., Andrews, J., et al. (1992). Evidence for massive discharges of icebergs into the north-Atlantic ocean during the last glacial period. *Nature*, *360*(6401), 245–249. https://doi.org/10.1038/360245a0

Boyle, E. D., & Keigwin, L. (1987). North Atlantic thermohaline circulation during the past 20,000 years linked to high-latitude surface temperature. *Nature*, *330*(6143), 35–40. https://doi.org/10.1038/330035a0

Brown, K. A., Williams, W. J., Carmack, E. C., Fiske, G., François, R., McLennan, D., & Peucker Ehrenbrink, B. (2020). Geochemistry of small canadian Arctic rivers with diverse geological and hydrological settings. *Journal of Geophysical Research: Biogeosciences*, *125*, e2019JG005414. https://doi.org/10.1029/2019JG005414

Burton, K. W., Abdelmouhcine, G., Birck, J.-L., Allègre, C. J., Schiano, P., Clocchiatti, R., & Alard, O. (2002). The compatibility of rhenium and osmium in natural olivine and their behavior during mantle melting and basalt genesis. *Earth and Planetary Science Letters*, *198*(1–2), 63–76. https://doi.org/10.1016/S0012-821X(02)00518-6

Came, R. E., Oppo, D. W., & Curry, W. B. (2003). Atlantic Ocean circulation during the younger dryas: Insights from a new Cd/Ca record from the western subtropical south Atlantic. *Paleoceanography*, *18*(4), 1086. https://doi.org/10.1029/2003PA000888

Chen, T. Y., Frank, M., Brian, A. H., Gutjahr, M., & Spielhagen, R. F. (2012). Variations of north Atlantic inflow to the central Arctic Ocean over the last 14 million years inferred from hafnium and neodymium isotopes. *Earth and Planetary Science Letters*, *353–354*, 82–92. https://doi.org/10.1016/j.epsl.2012.08.012

Chierici, M., & Fransson, A. (2009). Calcium carbonate saturation in the surface water of the Arctic Ocean: Under saturation in freshwater influenced shelves. *Biogeosciences*, *6*, 2421–2432. https://doi.org/10.5194/bg-6-2421-2009

Chikamoto, M. O., Matsumoto, K., & Ridgwell, A. (2008). Response of deep-sea $CaCO_3$ sedimentation to Atlantic meridional overturning circulation shutdown. *Journal of Geophysical Research*, *113*, G03017. https://doi.org/10.1029/2007JG000669

Codling, P. (2017). *Late quaternary ice sheet dynamics and palaeoceanography in the Ban Bay region*. Durham University. Retrieved from Durham E-theses online: http://etheses.dur.ac.uk/12676/

Cousens, B. L., Aspler, L. B., & ChiarenzelliJ, R. (2004). Dual sources of ensimatic magmas, hearne domain, western churchill province, nunavut, Canada: Neoarchean infant arc processes? *Precambrian Research*, *134*, 169–188. https://doi.org/10.1016/j.precamres.2004.06.001

Dausmann, V., Gutjahr, M., Frank, M., Kouzmanov, K., & Schaltegger, U. (2019). Experimental evidence for a mineral-controlled release of radiogenic Nd, Hf, and Pb isotopes from granitic rocks during progressive chemical weathering. *Chemical Geology*, *507*, 64–84. https://doi.org/10.1016/j.chemgeo.2018.12.024

Deike, R. G. (1990). Dolomite dissolution rates and possible holocene dedolomitization of water-bearing units in the edwards aquifer, south-central Texas. *Journal of Hydrology*, *112*, 335–373. https://doi.org/10.1016/0022-1694(90)90023-Q

Denton, G. H., & Hughes, T. (1981). *The last great ice sheet*s (pp. 484). Wiley-Interscience.

Dewing, K., Turner, E., & Harrison, J. C. (2007). Geological history, mineral occurrences and mineral potential of the sedimentary rocks of the canadian Arctic archipelago. In W. D. Goodfellow (Ed.), *Mineral deposits of Canada: A synthesis of major deposit-types, district metallogeny, the evolution of geological provinces, and exploration methods: Geological association of Canada* (Vol. 5, pp. 733–753). Mineral Deposits Division, Special Publication.

Dickson, R. R., & Brown, J. (1994). The production of north Atlantic deep water: Sources, rates, and pathways. *Journal of Geophysical Research*, *99*(C6), 12319–12341. https://doi.org/10.1029/94JC00530

Dickson, R. R., Meincke, J., Malmberg, S.-A., & Lee, A. J. (1988). The "great salinity anomaly" in the northern north Atlantic 1968–1982. *Progress in Oceanography*, *20*, 10–31. https://doi.org/10.1016/0079-6611(88)90049-3

Dommenget, D., & Latif, M. (2002). Analysis of observed and simulated SST spectra in the midlatitudes. *Climate Dynamic*s, *19*, 277–288. https://doi.org/10.1007/s00382-002-0229-9

Drever, J. I. (1997). *The geochemistry of natural waters: Surface and groundwater environment*s (pp. 436). Prentice-Hall.

Duplessy, J. C., Shackleton, N. J., Fairbanks, R. G., Labeyrie, L., Oppo, D., & Kallel, N. (1988). Deepwater source variations during the last climatic cycle and their impact on the global deepwater circulation. *Paleoceanography*, *3*(3), 343–360. https://doi.org/10.1029/PA003i003p00343

Dyke, A. S. (1999). Last glacial maximum and deglaciation of devon Island, Arctic Canada: Support for an innuitian ice sheet. *Quaternary Science Reviews*, *18*(3), 393–420. https://doi.org/10.1016/s0277-3791(98)00005-5

Dyke, A. S., Andrews, J. T., Clark, P. U., England, J. H., Miller, G. H., Shaw, J., & Veillette, J. J. (2002). The laurentide and innuitian ice sheets during the last glacial maximum. *Quaternary Science Reviews*, *21*(1), 9–31. https://doi.org/10.1016/s0277-3791(01)00095-6

Dyke, L. M., Hughes, A. L. C., Murray, T., Hiemstra, J. F., Andresen, C. S., & Rodes, A. (2014). Evidence for the asynchronous retreat of large outlet glaciers in southeast Greenland at the end of the last glaciation. *Quaternary Science Reviews*, *99*, 244–259. https://doi.org/10.1016/j.quascirev.2014.06.001

Elderfield, H., & Sholkovitz, E. R. (1987). Rare earth elements in the pore waters of reducing nearshore sediments. *Earth and Planetary Science Letters*, *82*, 280–288. https://doi.org/10.1016/0012-821X(87)90202-0

England, J. (1999). Coalescent Greenland and innuitian ice during the last glacial maximum: Revising the quaternary of the Canadian high Arctic. *Quaternary Science Reviews*, *18*(3), 421–456. https://doi.org/10.1016/s0277-3791(98)00070-5

England, J., Atkinson, N., Bednarski, J., Dyke, A. S., Hodgson, D. A., & Ó Cofaigh, C. (2006). The innuitian ice sheet: Configuration, dynamics and chronology. *Quaternary Science Reviews*, *25*(7– 8), 689–703. https://doi.org/10.1016/j.quascirev.2005.08.007

Ezat, M., Rasmussen, T., Hönisch, B., Groeneveld, J., & De Menocal, P. (2017). Episodic release of CO_2 from the high-latitude north Atlantic Ocean during the last 135 kyr. *Nature Communications*, *8*, 14498. https://doi.org/10.1038/ncomms14498

Fagel, N., Robert, C., & Hillaire-Marcel, C. (1996). Clay mineral signature of the NW atlantic boundary undercurrent. *Marine Geology*, *130*(1), 19–28. https://doi.org/10.1016/0025-3227(95)00134-4

Fagel, N., Hillaire-Marcel, C., & Robert, C. (1997). Changes in the western boundary undercurrents outflow since the last glacial maximum, from smectite/illite ratios in deep Labrador Sea sediments. *Paleoceanography*, *12*(1), 79–96. https://doi.org/10.1029/96pa02877

Fagel, N., Hillaire-Marcel, C., Humbelt, M., Brasseur, R., Weis, D., & Stevenson, R. (2004). Nd and Pb isotope signatures of the clay-size fraction of Labrador Sea sediments during the Holocene: Implications for the inception of the modern deep circulation pattern. *Paleoceanography*, *9*. https://doi.org/10.1029/2003PA000993

Fagel, N., Innocent, C., Ariepy, C., & Hillaire-Marcel, C. (2002). Sources of Labrador Sea sediments since the last glacial maximum inferred from Nd-Pb isotopes. *Geochimica et Cosmochimica Acta*, *66*, 2569–2581. https://doi.org/10.1016/s0016-7037(02)00866-9

Fagel, N., Innocent, C., Stevenson, K., & Hillaire-Marcel, C. (1999). Deep circulation changes in the Labrador Sea since the last glacial maximum: New constraints from Sm-Nd data on sediments. *Paleoceanography*, *14*(6), 777–788. https://doi.org/10.1029/1999pa900041

Filippova, A. (2016). Reconstruction of the water mass circulation patterns in the Labrador Sea based on radiogenic isotopes and alkenone composition from the present day up to the late quaternary (35 kyrs). PhD Thesis Retrieved from https://oceanrep.geomar.de/id/eprint/35354/1/Filippova_%20Thesis.pdf

Filippova, A., Frank, M., Kienast, M., Gutjahr, M., Hathorne, Ed, C., et al. (2022). Radiogenic Nd isotope signatures and REE concentrations of marine sediments (bulk and detrital), foraminifera and dolostone grains from 4 sediment downcore records from the Labrador Sea. PANGAEA. https://doi.org/10.1594/PANGAEA.952659

Fisher, J., Visbeck, M., Zantopp, R., & Nunes, N. (2010). Interannual to decadal variability of outflow from the Labrador Sea. *Geophysical Research Letters*, *37*, L24610. https://doi.org/10.1029/2010GL045321

Frank, M. (2002). Radiogenic isotopes: Tracers of past ocean circulation and erosional input. *Reviews of Geophysics*, *40*, 1001. https://doi.org/10.1029/2000RG000094

Funder, S., & Hansen, L. (1996). The Greenland ice sheet—A model for its culmination and decay during and after the last glacial maximum. *Bulletin of the Geological Society of Denmark*, *42*(2), 137–152. https://doi.org/10.1029/2000rg000094

Funder, S., Jennings, A. E., & Kelly, M. J. (2004). Middle and late quaternary glacial limits in Greenland. In J. Ehlers & P. L. Gibbard (Eds.), *Quaternary glaciations-extent and chronology, Part II* (pp. 425–430). Elsevier. https://doi.org/10.1016/s1571-0866(04)80210-0

Gibb, O. T., Hillaire-Marcel, C., & De Vernal, A. (2014). Oceanographic regimes in the northwest Labrador Sea since marine isotope stage 3 based on dinocyst and stable isotope proxy records. *Quaternary Science Reviews*, *92*, 269–279. https://doi.org/10.1016/j.quascirev.2013.12.010

Grenier, M., Brown, K. A., Colombo, M., Belhadj, M., Baconnais, I., Pham, V., et al. (2022). Controlling factors and impacts of river-borne neodymium isotope signatures and rare earth element concentrations supplied to the canadian Arctic archipelago. *Earth and Planetary Science Letters*, *578*, 117341. https://doi.org/10.1016/j.epsl.2021.117341

Gulev, S. K., Zolina, O., & Grigoriev, S. (2001). Extratropical cyclone variability in the Northern Hemisphere winter from the NCEP/NCAR reanalysis data. *Climate Dyamic*, *17*, 795–809. https://doi.org/10.1007/s003820000145

Gutjahr, M., Frank, M., Stirling, C. H., Keigwin, L. D., & Halliday, A. N. (2008). Tracing the Nd isotope evolution of north Atlantic deep and intermediate waters in the western north Atlantic since the last glacial maximum from Blake ridge sediments. *Earth and Planetary Science Letters*, *266*, 61–77. https://doi.org/10.1016/j.epsl.2007.10.037

Gutjahr, M., Frank, M., Stirling, C. H., Klemm, V., Van de Flierdt, T., & Halliday, A. N. (2007). Reliable extraction of a deepwater trace metal isotope signal from Fe-Mn oxyhydroxide coatings of marine sediments. *Chemical Geology*, *242*, 351–370. https://doi.org/10.1016/j.chemgeo.2007.03.021

Haflidason, H., Eiriksson, J., & Kreveld, S. V. (1999). The tephrochronology of Iceland and north Atlantic region during the middle and late quaternary: A review journal of. *Quaternary Sciences*, *15*, 3–22.

Haley, B. A., Klinkhammer, G. P., & McManus, J. (2004). Rare earth elements in pore waters of marine sediments. *Geochimica et Cosmochimica Acta*, *68*, 1265–1279. https://doi.org/10.1016/j.gca.2003.09.012

Hall, A., & Qu, X. (2006). Using the current seasonal cycle to constrain snow albedo feedback in future climate change. *Geophysical Research Letters*, *33*, L03502. https://doi.org/10.1029/2005GL025127

Haskell, B. J., Johnson, T. C., & Showers, W. J. (1991). Fluctuations in deep western north Atlantic circulation on the blake outer ridge during the last deglaciation. *Paleoceanography*, *6*(1), 21–31. https://doi.org/10.1029/90PA01939

Heaton, T., Köhler, P., Butzin, M., Bard, E., Reimer, R., Austin, W., et al. (2020). Marine20—The marine radiocarbon age calibration curve (0–55,000 cal BP). *Radiocarbon*, *62*(4), 779–820. https://doi.org/10.1017/RDC.2020.68

Hecht, L., Freiberger, R., Gilg, H. A., Grundmann, G., & Kostitsyn, Y. (1999). Rare element and isotope C, O, Sr characteristics of hydrothermal carbonates: Genetic implications for dolomite-hosted talc mineralization at gopfersgrun (Fichtelgebirge, Germany). *Chemical Geology*, *155*, 115–130. https://doi.org/10.1016/s0009-2541(98)00144-2

Heinrich, H. (1988). Origin and consequences of cyclic ice rafting in the northeast Atlantic Ocean during the past 130,000 years. *Quaternary Research*, *29*, 142–152. https://doi.org/10.1016/0033-5894(88)90057-9

Hemming, S. R. (2004). Heinrich events: Massive late Pleistocene detritus layers of the north Atlantic and their global climate imprint. *Review of Geophysics*, *42*, RG1005. https://doi.org/10.1029/2003RG000128

Hemming, S. R., Broecker, W. S., Sharp, W. D., Bond, G. C., Gwiazda, R. H., McManus, J. F., et al. (1998). Provenance of heinrich layers in core V28-82, northeastern atlantic: 40Ar=39Ar ages of ice-rafted hornblende, Pb isotopes in feldspar grains, and Nd–Sr–Pb isotopes in the fine sediment fraction. *Earth and Planetary Science Letters*, *164*, 317–333. https://doi.org/10.1016/s0012-821x(98)00224-6

Hesse, R., & Khodabakhsh, S. (2006). Significance of fine-grained sediment lofting from melt-water generated turbidity currents for the timing of glaciomarine sediment transport into the deep sea. *Sedimentary Geology*, *186*, 1–11. https://doi.org/10.1016/j.sedgeo.2005.10.006

Hesse, R., & Khodabakhsh, S. (2016). Anatomy of Labrador Sea heinrich layers. *Marine Geology*, *380*, 44–66. https://doi.org/10.1016/j.margeo.2016.05.019

Hesse, R., Rashid, H., & Khodabakhsh, S. (2004). Fine-grained sediment lofting from meltwater-generated turbidity currents during heinrich events. *Geology*, *32*, 449–452. https://doi.org/10.1130/g20136.1

Hillaire-Marcel, C., & De Vernal (1989). Lsotopic and palynological records of the late Pleistocene in eastern Canada and adjacent ocean basins. *Géographie Physique et Quaternaire*, *43*(3), 263–290.

Hillaire-Marcel, C., De Vernal, A., Bilodeau, G., & Wu, G. (1994). Isotope stratigraphy, sedimentation rates and paleoceanographic changes in the Labrador Sea. *Canadian Journal of Earth Sciences*, *31*, 63–89. https://doi.org/10.1139/e94-007

Hillaire-Marcel, C., De Vernal, A., & Piper, D. J. W. (2007). Lake Agassiz final drainage event in the northwest north Atlantic. *Geophysical Research Letters*, *34*(15), L15601. https://doi.org/10.1029/2007GL030392007

Howe, J., Piotrowski, A., Noble, T., Mulitza, S., Chiessi, C. M., & Bayon, G. (2016). North Atlantic deep water production during the last glacial maximum. *Nature Communications*, *7*, 11765. https://doi.org/10.1038/ncomms11765

Howe, J. N. W., Huang, K.-F., Oppo, D. W., Chiessi, C. M., Mulitza, S., Blusztajn, J., & Piotrowski, A. M. (2018). Similar mid-depth atlantic water mass provenance during the last glacial maximum and heinrich stadial 1. *Earth and Planetary Science Letters*, *490*, 51–61. https://doi.org/10.1016/j.epsl.2018.03.006

Howe, J. N. W., Piotrowski, A. M., Oppo, D. W., Huang, K.-F., Mulitza, S., Chiessi, C. M., & Blusztajn, J. (2016). Antarctic intermediate water circulation in the south Atlantic over the past 25,000 years. *Paleoceanography*, *31*, 1302–1314. https://doi.org/10.1002/2016PA002975

Howe, J. N. W., Piotrowski, A. M., & Rennie, V. C. F. (2016). Abyssal origin for the early holocene pulse of unradiogenic neodymium isotopes in Atlantic seawater. *Geology*, *44*, 831–834. https://doi.org/10.1130/g38155.1

Huang, H., Gutjahr, M., Eisenhauer, A., & Kuhn, G. (2020). No detectable weddell sea Antarctic bottom water export during the last and Penultimate glacial maximum. *Nature Communications*, *11*, 424. https://doi.org/10.1038/s41467-020-14302-3

Huang, K.-F., Oppo, D. W., & Curry, W. B. (2014). Decreased influence of Antarctic intermediate water in the tropical Atlantic during north Atlantic cold even ts. *Earth and Planetary Science*, *389*, 208. https://doi.org/10.1016/j.epsl.2013.12.037

Innocent, C., Fagel, N., & Hillaire-Marcel, C. (2000). Sm–Nd isotope systematics in deep-sea sediments: Clay-size versus coarser fractions. *Marine Geology*, *168*(1), 79–87. https://doi.org/10.1016/S0025-3227(00)00052-9

Innocent, C., Fagel, N., Stevenson, R. K., & Hillaire-Marcel, C. (1997). Sm-Nd signature of modern and late quaternary sediments from the northwest north Atlantic: Implications for deep current changes since the last glacial maximum. *Earth and Planetary Science Letters*, *146*, 607–625. https://doi.org/10.1016/s0012-821x(96)00251-8

Jackson, R., Carlson, A. E., Hillaire-Marcel, C., Wacker, L., Vogt, C., & Kucera, M. (2017). Asynchronous instability of the north American-Arctic and Greenland ice sheets during the last deglaciation. *Quaternary Science Reviews*, *164*(140), 140–153. https://doi.org/10.1016/j.quascirev.2017.03.020

Jacobsen, S. B., & Wasserburg, G. J. (1980). Sm-Nd isotopic evolution of chondrites. *Earth and Planetary Science Letter*s, *50*, 139–155. https://doi.org/10.1016/0012-821x(80)90125-9

Jaume-Seguí, M., Kim, J., Pena, L. D., Goldstein, S. L., Knudson, K. P., Yehudai, M., et al. (2020). Distinguishing glacial AMOC and interglacial non-AMOC Nd isotopic signals in the deep western atlantic over the last 1 Myr. *Paleoceanography and Paleoclimatology*, *36*, e2020PA003877. https://doi.org/10.1029/2020PA003877

Jeandel, C. (2016). Overview of the mechanisms that could explain the "boundary exchange" at the land–ocean contact. *Philosophical Transactions of the Royal Society A*, *374*, 20150287. https://doi.org/10.1098/rsta.2015.0287

Jennings, A. E., Hald, M., Smith, M., & Andrews, J. T. (2006). Freshwater forcing from the Greenland ice sheet during the younger dryas: Evidence from southeastern Greenland shelf cores. *Quaternary science review*, *25*, 282–298. https://doi.org/10.1016/j.quascirev.2005.04.006

Kah, L. C., Sherman, A. G., Narbonne, G. M., Knoll, A. H., & Kaufmand, A. J. (1999). 13C stratigraphy of the Proterozoic bylot supergroup, Baffin Island, Canada: Implications for regional lithostratigraphic correlations. *Canadian Journal of Earth Sciences*, *36*, 313–332. https://doi.org/10.1139/e98-100

Keigwin, L. D., & Swift, S. A. (2017). Carbon isotope evidence for a northern source of deep water in the glacial western north Atlantic. *Proceedings of the National Academy of Sciences*, *114*(11), 2831–2835. https://doi.org/10.1073/pnas.1614693114

Khatiwala, S., Schlosser, P., & Visbeck, M. (2002). Rates and mechanisms of water mass transformation in the Labrador Sea as inferred from tracer observations. *Journal of Physical Oceanography*, *32*(2), 666–686. https://doi.org/10.1175/1520-0485(2002)032<0666:ramowm>2.0.co;2

Khodabakhsh, S. (1997). Ph.D. Thesis Pleistocene laurentide ice sheet drainage into the Labrador Sea: Sedimentary facies, depositional mechanisms, stratigraphy and significance of Heinrich events (pp. 263). Unpublished McGill University.

Kieke, D., & Yashayaev, I. (2014). Studies of Labrador Sea water formation and variability in the subpolar North Atlantic in the light of international partnership and collaboration. *Progress in Oceanography*, *132*, 202–232. https://doi.org/10.1016/j.pocean.2014.12.010

Kirillova, V. (2017). *Radiogenic isotopes on marine sediments from the Baffin Bay: Implications for the sediment supply during the last deglaciation*. Dissertation, University of Bremen.

Kučera, J., Cempírek, J., Dolníček, Z., Muchez, P., & Prochaska, W. (2009). Rare earth elements and yttrium geochemistry of dolomite from post-Variscan vein-type mineralization of the Nízký Jeseník and upper silesian basins, Czech Republic. *Journal of Geochemical Exploration*, *103*, 69–79.

Kuebler, C., Simonetti, A., Chen, W., & Simonetti, S. S. (2020). Boron isotopic investigation of the Bayan Obo carbonatite complex: Insights into the source of mantle carbon and hydrothermal alteration. *Chemical Geology*, *557*, 119859. https://doi.org/10.1016/j.chemgeo.2020.119859

Lacan, F., & Jeandel, C. (2005). Acquisition of the neodymium isotopic composition of the north Atlantic deep water. *Geochemistry Geophyics. Geosystems*, *6*(12), Q12008. https://doi.org/10.1029/2005GC000956

Lambelet, M., Van de Flierdt, T., Crocket, K., Rehkamper, M., Kreissig, K., Coles, B., et al. (2016). Neodymium isotopic composition and concentration in the western North Atlantic ocean: Results from the geotraces GA02 section. *Geochimica et Cosmochimica Acta*, *177*, 1–29. https://doi.org/10.1016/j.gca.2015.12.019

Langmuir, D. (1997). *Aqueous environmental geochemistry* (pp. 600). Prentice-Hall.

Lavoie, D., Zhang, S., & Pinet, N. (2011). Hydrothermal dolomites in Hudson Bay platform and southeast Arctic platform: Preliminary field and geochemical data. *Geological survey of Canada, open file 7002*, 19. https://doi.org/10.4095/289303

Lazier, J. R. N. (1980). Oceanographic conditions at ocean weather ship Bravo, 1964–1974. *Atmosphere-Ocean*, *18*(3), 227–238. https://doi.org/10.1080/07055900.1980.9649089

Lazier, J. R. N., & Wright, D. G. (1993). Annual velocity variations in the Labrador current. *Journal of Physical Oceanography*, *23*, 659–678. https://doi.org/10.1175/1520-0485(1993)023<0659:avvitl>2.0.co;2

Le Bas, M., Xueming, Y., Taylor, R., Spiro, B., Milton, J. A., & Peishan, Z. (2007). New evidence from a calcite-dolomite carbonatite dyke for the magmatic origin of the massive Bayan Obo ore-bearing dolomite marble, inner Mongolia, China. *Mineralogy and Petrology*, *90*, 223–248. https://doi.org/10.1007/s00710-006-0177-x

Ledbetter, M. T., & Balsam, W. L. (1985). Paleoceanography of the deep western boundary undercurrent on the North American continental margin for the past 25,000 yr. *Geology*, *13*(3), 181–184. https://doi.org/10.1130/0091-7613(1985)13<181:potdwb>2.0.co;2

Lewis, C. F. M., Miller, A. A. L., Levac, E., Piper, D. J. W., & Sonnichsen, G. V. (2011). Lake Agassiz outburst age and routing by Labrador current and the 8.2 cal ka cold event. *Quaternary International*, *260*, 83–97. https://doi.org/10.1016/j.quaint.2011.08.023

Lippold, J., Gutjahr, M., Blaser, P., Christner, E., De Carvalho Ferreira, M. L., Mulitza, S., et al. (2016). Deep water provenance and dynamics of the (de)glacial Atlantic meridional overturning circulation. *Earth and Planetary Science Letters*, *445*, 68–78. https://doi.org/10.1016/j.epsl.2016.04.013

Lochte, A. A., Repschläger, J., Kienast, M., Schönberg, D. B., Andersen, N., Hamann, C., & Schneider, R. (2019). Labrador Sea freshening at 8.5 ka BP caused by Hudson Bay ice saddle collapse. *Nature Communications*, *10*, 586. https://doi.org/10.1038/s41467-019-08408-6

Lochte, A. A., Repschläger, J., Seidenkrantz, M.-S., Kienast, M., Blanz, T., & Schneider, R. R. (2019). Holocene water mass changes in the Labrador current. *The Holocene*, *29*(4), 676–690. https://doi.org/10.1177/0959683618824752

Lucotte, M., & Hillaire-Marcel, C. (1994). Identification et distribution des grandes masses d'eau dans les mers du Labrador et d'Irminger. *Canadian Journal of Earth Sciences*, *31*(1), 5–13. https://doi.org/10.1139/e94-002

MacLean, B., Williams, G. L., Jennings, A. E., & Blakeney, C. (1986). *Cumberland sound, N.W.T: Investigations of bedrock and surficial geology*. Geological survey of Canada. paper 86-1 B, 605–616.

Margold, M., Stokes, C. R., & Clark, C. D. (2015). Ice streams in the laurentide ice sheet: Identification, characteristics and comparison to modern ice sheets. *Earth-Science Reviews*, *143*, 117–146. https://doi.org/10.1016/j.earscirev.2015.01.011

Margold, M., Stokes, C. R., & Clark, C. D. (2018). Reconciling records of ice streaming and ice margin retreat to produce a palaeogeographic reconstruction of the deglaciation of the laurentide ice sheet. *Quaternary Science Reviews*, *189*, 1–30. https://doi.org/10.1016/j.quascirev.2018.03.013

Marshall, N. R., De Vernal, A., Mucci, A., Filippova, A., Kienast, M., Gibb, O., & Hillaire-Marcel, C. (2021). Biogenic carbonate fluxes and preservation in the northwestern Labrador Sea since the last glacial maximum. *Palaeogeography, Palaeoclimatology, Palaeoecology*, *576*, 110498. https://doi.org/10.1016/j.palaeo.2021.110498

Martin, E. E., Blair, S. W., Kamenov, G. D., Scher, H. D., Bourbon, E., Basak, C., & Newkirk, D. N. (2010). Extraction of Nd isotopes from bulk deep sea sediments for paleoceanographic studies on Cenozoic time scales. *Chemical Geology*, *269*, 414–431. https://doi.org/10.1016/j.chemgeo.2009.10.016

Mathieu, J., Turner, E. C., & Rainbird, R. H. (2013). *Sedimentary architecture of a deeply karsted precambrian–cambrian unconformity, Victoria Island, northwest territories*. Geological Survey of Canada Current Research.

McCarthy, G. D., Haigh, I. D., Hirschi, J. J.-M., Grist, J. P., & Smeed, D. A. (2015). Ocean impact on decadal-scale Atlantic climate variations revealed by sea-level observations. *Nature*, *521*, 508–510. https://doi.org/10.1038/nature14491

McLennan, S. (2001). Relationship between the trace element composition of sedimentary rocks and upper continental crust. *Geochemistry, Geophysics, Geosystems*, *2*, 4. https://doi.org/10.1029/2000GC000109

McManus, J., Francois, R., Gherardi, J., Keigwin, L. D., & Brown-Leger, S. (2004). Collapse and rapid resumption of Atlantic meridional circulation linked to deglacial climate changes. *Nature*, *428*, 834–837. https://doi.org/10.1038/nature02494

Meredyk, S. P., Edinger, E., Piper, D. J. W., Huvenne, V. A. I., Hoy, S., & Ruffman, A. (2020). Enigmatic deep-water mounds on the Orphan Knoll, Labrador Sea. *Frontiers in Marine Science*, *6*, 744. https://doi.org/10.3389/fmars.2019.00744

Moros, M., Andrews, J. T., Eberl, D., & Jansen, E. (2006). Holocene history of drift ice in the northern North Atlantic: Evidence for different spatial and temporal mode. *Paleoceanography*, *21*, PA2017. https://doi.org/10.1029/2005PA001214

Moros, M., Jansen, E., Oppo, D. W., Giraudeau, J., & Kuijpers, A. (2012). Reconstruction of the late-holocene changes in the sub-Arctic front position at the Reykjanes Ridge, North Atlantic. *The Holocene*, *22*(8), 877–886. https://doi.org/10.1177/0959683611434224

Nuttin, L., Maccali, J., & Hillaire-Marcel, C. (2015). U, Th, and Pa insights into sedimentological and paleoceanographic changes off Hudson Strait (Labrador Sea) during the last ~37 ka with special attention to methodological issues. *Quaternary Science Reviews*, *115*, 39–49. https://doi.org/10.1016/j.quascirev.2015.02.015

Oksman, M., Weckström, K., Miettinen, A., Juggins, S., Divine, D. V., Jackson, R., et al. (2017). Younger dryas ice margin retreat triggered by ocean surface warming in central-eastern Baffin Bay. *Nature Communications*, *8*, 1017. https://doi.org/10.1038/s41467-017-01155-6

Oppo, D. W., & Fairbanks, R. G. (1987). Variability in the deep and intermediate water circulation of the Atlantic during the past 25,000 years: Northern Hemisphere modulation of the Southern Ocean. *Earth Planetary Science*, *86*, 1–15. https://doi.org/10.1016/0012-821x(87)90183-x

Pahnke, K., Goldstein, S. L., & Hemming, S. (2008). Abrupt changes in Antarctic intermediate water circulation over the past 25,000 years. *Nature Geoscience*, *1*, 870–874. https://doi.org/10.1038/ngeo360

Patton, G. M., Francois, R., Weis, D., Hathorne, E., Gutjahr, M., Frank, M., & Gordon, K. (2021). An experimental investigation of the acquisition of Nd by authigenic phases of marine sediments. *Geochimica et Cosmochimica Acta*, *301*, 1–29. https://doi.org/10.1016/j.gca.2021.02.010

Perner, K., Moros, M., Jennings, A., Lloyd, J. M., & Knudsen, K. L. (2012). *Holocene palaeoceanographic evolution off west Greenland the holocene*, *23*(3), 374–387. https://doi.org/10.1177/0959683612460785

Pin, C., & Zalduegui, J. S. (1997). Sequential separation of light rare-earth elements, thorium and uranium by miniaturized extraction chromatography: Application to isotopic analyses of silicate rocks. *Analytica Chemica Acta*, *339*, 79–89. https://doi.org/10.1016/s0003-2670(96)00499-0

Pöppelmeier, F., Blaser, P., Gutjahr, M., Jaccard, S. L., Frank, M., Max, L., & Lippold, J. (2020). Northern-sourced water dominated the Atlantic Ocean during the last glacial maximum. *Geology*, *48*, 826–829. https://doi.org/10.1130/G47628.1

Pöppelmeier, F., Gutjahr, M., Blaser, P., Keigwin, L. D., & Lippold, J. (2018). Origin of abyssal NW atlantic water masses since the last glacial maximum. *Paleoceanography and Paleoclimatology*, *33*(5), 530–543. https://doi.org/10.1029/2017PA003290

Pöppelmeier, F., Lippold, J., Blaser, P., Gutjahr, M., Frank, M., & Stocker, T. F. (2022). Neodymium isotopes as a paleo-water mass tracer: A model-data reassessment. *Quaternary Science Reviews*, *279*, 107404.

Rainsley, E., Menviel, L., Fogwill, C. J., Turney, C. S. M., Hughes, A. L. C., & Rood, D. H. (2018). Greenland ice mass loss during the younger dryas driven by atlantic meridional overturning circulation feedbacks. *Scientific Reports*, *8*, 11307. https://doi.org/10.1038/s41598-018-29226-8

Rashid, H., Saint-Ange, F., Barber, D. C., Smith, M. E., & Devalia, N. (2012). Fine scale sediment structure and geochemical signature between eastern and western north Atlantic during heinrich events 1 and 2. *Quaternary Science Reviews*, *46*, 136–150. https://doi.org/10.1016/j.quascirev.2012.04.026

Rempfer, J., Stocker, T. F., Joos, F., Dutay, J. C., & Siddall, M. (2011). Modelling Nd-isotopes with a coarse resolution ocean circulation model: Sensitivities to model parameters and source/sink distributions. *Geochimica et Cosmochimica Acta*, *75*(20), 5927–5950. https://doi.org/10.1016/j.gca.2011.07.044

Roberts, N. L., & Piotrowski, A. M. (2015). Radiogenic Nd isotope labeling of the northern NE Atlantic during MIS 2. *Earth and Planetary Science Letters*, *423*, 125–133. https://doi.org/10.1016/j.epsl.2015.05.011

Roberts, N. L., Piotrowski, A. M., McManus, J. F., & Keigwin, L. D. (2010). Synchronous deglacial overturning and water mass source changes. *Science*, *327*, 75–78. https://doi.org/10.1126/science.1178068

Roberts, W. H. G., Valdes, P. J., & Payne, A. J. (2014). A new constraint on the size of heinrich events from an iceberg/sediment model. *Earth and Planetary Science Letters*, *386*, 1–9. https://doi.org/10.1016/j.epsl.2013.10.020

Sandeman, H. A., Hanmer, S., Davis, W. J., RyanJ, J., & Peterson, T. D. (2004). Neoarchaean volcanic rocks, central hearne supracrustal belt, western churchill province, Canada: Geochemical and isotopic evidence supporting intra-oceanic supra-subduction zone extension. *Precambrian Research*, *134*, 113–141. https://doi.org/10.1016/j.precamres.2004.03.014

Sandeman, H. A., Hanmer, S., Tella, S., Armitage, A. A., Davis, W. J., & Ryan, J. J. (2006). Petrogenesis of neoarchaean volcanic rocks of the macquoid supracrustal belt: A back-arc setting for the northwestern hearne subdomain, western churchill province, Canada. *Precambrian Research*, *144*, 140–165. https://doi.org/10.1016/j.precamres.2005.11.001

Schlitzer, R. (2015). *Ocean data view*. odv.awi.de.

Seidenkrantz, M.-S., Kuijpers, A., Aagaard-Sorensen, S., Lingreen, H., Olsen, J., & Pearce, C. (2021). Evidence for influx of atlantic water masses to the Labrador Sea during the last glacial maximum. *Scientific Reports*. https://doi.org/10.1038/s41598-021-86224-z

Simon, Q., Hillaire-Marcel, C., St-Onge, G., & Andrews, J. T. (2014). North-eastern Laurentide, western Greenland and southern innuitian ice stream dynamics during the last glacial cycle. *Journal of Quaternary Science*, *29*, 14–16. https://doi.org/10.1002/jqs.2648

Simon, Q., St-Onge, G., & Hillaire-Marcel, C. (2012). Late Quaternary chronostratigraphic framework of deep Baffin Bay glaciomarine sediments from high-resolution paleomagnetic data. *Geochemistry, Geophysics, Geosystems*, *13*(11), Q0AO03. https://doi.org/10.1029/2012GC004272

Smrzka, D., Zwicker, J., Bach, W., Feng, D., Himmler, T., Chen, D., & Peckmann, J. (2019). The behavior of trace elements in seawater, sedimentary pore water, and their incorporation into carbonate minerals: A review. *Facies*, *65*, 41. https://doi.org/10.1007/s10347-019-0581-4

Stuiver, M., & Reimer, P. J. (1993). CALIB rev. 8. *Radiocarbon*, *35*, 215–230. https://doi.org/10.1017/s0033822200013904

Szramek, K., McIntosh, J. C., Williams, E. L., Kanduc, T., Ogrinc, N., & Walter, L. M. (2007). Relative weathering intensity of calcite versus dolomite in carbonate-bearing temperate zone watersheds: Carbonate geochemistry and fluxes from catchments within the St. Lawrence and Danube river basins. *Geochemistry, Geophysics, Geosystems*, *8*, Q04002. https://doi.org/10.1029/2006GC001337

Tachikawa, K., Athias, V., & Jeandel, C. (2003). Neodymium budget in the modern ocean and paleo-oceanographic implications. *Journal of Geophysical Research*, *108*(C8). https://doi.org/10.1029/1999jc000285

Tachikawa, K., Piotrowski, A. M., & Bayon, G. (2014). Neodymium associated with foraminiferal carbonate as a recorder of seawater isotopic signatures. *Quaternary Science Reviews*, *88*, 1–13. https://doi.org/10.1016/j.quascirev.2013.12.027

Tanaka, T., Togashi, S., Kamioka, H., Amakawa, H., Kagami, H., Hamamoto, T., et al. (2000). JNdi-1: A neodymium isotopic reference in consistency with LaJolla neodymium. *Chemical Geology*, *168*(3–4), 279–281. https://doi.org/10.1016/s0009-2541(00)00198-4

Thiagarajan, N., Subhas, A., Southon, J. R., Eiler, J. M., & Adkins, J. F. (2014). Abrupt pre-Bølling–Allerød warming and circulation changes in the deep ocean. *Nature*, *511*, 75–78. https://doi.org/10.1038/nature13472

Thornalley, D. J. R., Bauch, H. A., Gebbie, G., Guo1, W., Ziegler, M., Bernasconi, S. M., et al. (2015). A warm and poorly ventilated deep Arctic mediterranean during the last glacial period. *Science*, *349*, 706–710. https://doi.org/10.1126/science.aaa9554

Trouet, V., Scourse, J. D., & Raible, C. C. (2012). North Atlantic storminess and atlantic meridional overturning circulation during the last millennium: Reconciling contradictory proxy records of NAO variability. *Global and Planetary Change*, *84–85*, 48–55. https://doi.org/10.1016/j.gloplacha.2011.10.003

Vance, D., & Thirlwall, M. (2002). An assessment of mass discrimination in MC-ICPMS using Nd isotopes. *Chemical Geology*, *185*, 227–240. https://doi.org/10.1016/S0009-2541(01)00402-8

Veiga-Pires, C. C., & Hillaire-Marcel, C. (1999). U and Th isotope constraints on the duration of Heinrich events H0-H4 in the southeastern Labrador Sea. *Paleoceanography*, *14*(2), 187–199. https://doi.org/10.1029/1998PA900003

Vellinga, M., & Wood, R. A. (2002). Global climatic impacts of a collapse of the Atlantic thermohaline circulation. *Climatic Change*, *54*, 251–267. https://doi.org/10.1023/a:1016168827653

Wang, R. Z., Huang, K., Zhang, D., Liu, X., Luo, W., & You, L. (2017). Rare earth element and yttrium (REY) geochemistry of Cenozoic carbonates on the Xuande Atoll of the Xisha Archipelago, the south China sea: Implications of the impact of dolomitization on. *Geochemical Journal*, *51*, 507–523. https://doi.org/10.2343/geochemj.2.0487

Weidick, A., Kelly, M., & Bennike, O. (2004). Later quaternary development of the southern sector of the Greenland ice sheet, with particular reference to the Qassimiut lobe. *Boreas*, *33*, 284–299.

Wheeler, J. O., Hoffman, P. F., Card, K. D., Davidson, A., Sanford, B. V., Okulitch, A. V., & Roest, W. R. (1996). Geological survey of canada, map series "A" 1860A. https://doi.org/10.4095/208175

Winsborrow, M. C. M., Clark, C. D., & Stokes, C. R. (2004). Ice streams of the Laurentide ice sheet. *Géographie Physique et Quaternaire*, *58*(2–3), 269–280.

Xie, R. C., Marcantonio, F., & Schmidt, M. W. (2012). Deglacial variability of Antarctic intermediate water penetration into the north Atlantic from authigenic neodymium isotope ratios. *Paleoceanography*, *27*, PA3221. https://doi.org/10.1029/2012PA002337

Xie, R. C., Marcantonio, F., & Schmidt, M. W. (2014). Recpnstruction of intermediate water circulation in the tropical north Atlantic during the past 22,000 kyr. *Geochimica et Cosmochimica Acta*, *140*, 455–467. https://doi.org/10.1016/j.gca.2014.05.041

Yang, X. Y., Sun, W.-D., Zhang, Y. X., & Zheng, Y.-F. (2009). Geochemical constraints on the genesis of the Bayan Obo Fe–Nb–REE deposit in inner Mongolia, China. *Geochimica et Cosmochimica Acta*, *73*, 1417–1435. https://doi.org/10.1016/j.gca.2008.12.003

Yashayaev, I., & Clark, A. (2006). Recent warming of the Labrador Sea. *AZMP Bulletin PMZA*, *5*, 12–20.

Yashayaev, I., & Loder, J. W. (2009). Enhanced production of Labrador Sea water in 2008. *Geophysical Research Letters*, *36*, L01606. https://doi.org/10.1029/2008GL036162

Yashayaev, I., & Loder, J. W. (2016). Recurrent replenishment of Labrador Sea water and associated decadal-scale variability. *Journal of Geophysical Research–Oceans*, *121*, 8095–8114. https://doi.org/10.1002/2016JC012046

Yu, J., Menviel, L., Jin, Z. D., Thornalley, D. J. R., Foster, G. L., Rohling, E. J., et al. (2019). More efficient north Atlantic carbon pump during the last glacial maximum. *Nature Communications*, *10*, 2170. https://doi.org/10.1038/s41467-019-10028-z

Zhao, N., Oppo, D. W., Huang, K., Howe, J. N. W., Blusztajn, J., & Keigwin, L. D. (2019). Glacial–interglacial Nd isotope variability of north Atlantic deep water modulated by north American ice sheet. *Nature Communications*, *10*, 5773. https://doi.org/10.1038/s41467-019-13707-z